Monthly Notices
of the
ROYAL ASTRONOMICAL SOCIETY

MNRAS **493,** 4186–4208 (2020)
Advance Access publication 2020 February 19

doi:10.1093/mnras/staa499

The ASAS-SN catalogue of variable stars VI: an all-sky sample of δ Scuti stars

T. Jayasinghe [1,2]★ K. Z. Stanek,[1,2] C. S. Kochanek,[1,2] P. J. Vallely [1,2] B. J. Shappee,[3] T. W.-S. Holoien [4] Todd A. Thompson,[1,2,5] J. L. Prieto,[6,7] O. Pejcha [8] M. Fausnaugh,[9] S. Otero,[10] N. Hurst[11] and D. Will[1,11]

[1]*Department of Astronomy, The Ohio State University, 140 West 18th Avenue, Columbus, OH 43210, USA*
[2]*Center for Cosmology and Astroparticle Physics, The Ohio State University, 191 W. Woodruff Avenue, Columbus, OH 43210, USA*
[3]*Institute for Astronomy, University of Hawaii, 2680 Woodlawn Drive, Honolulu, HI 96822, USA*
[4]*Carnegie Observatories, 813 Santa Barbara Street, Pasadena, CA 91101, USA*
[5]*Institute for Advanced Study, Princeton, NJ 08540, USA*
[6]*Núcleo de Astronomía de la Facultad de Ingeniería y Ciencias, Universidad Diego Portales, Av. Ejército 441, Santiago, Chile*
[7]*Millennium Institute of Astrophysics, Santiago, Chile*
[8]*Institute of Theoretical Physics, Faculty of Mathematics and Physics, Charles University, Czech Republic*
[9]*MIT Kavli Institute for Astrophysics and Space Research, 77 Massachusetts Avenue, 37-241, Cambridge, MA 02139, USA*
[10]*The American Association of Variable Star Observers, 49 Bay State Road, Cambridge, MA 02138, USA*
[11]*ASC Technology Services, 433 Mendenhall Laboratory, 125 South Oval Mall, Columbus, OH 43210, USA*

Accepted 2020 February 17. Received 2020 February 13; in original form 2019 October 30

ABSTRACT

We characterize an all-sky catalogue of ∼8400 δ Scuti variables in ASAS-SN, which includes ∼3300 new discoveries. Using distances from *Gaia* DR2, we derive period–luminosity relationships for both the fundamental mode and overtone pulsators in the W_{JK}, V, *Gaia* DR2 G, J, H, K_s, and W_1 bands. We find that the overtone pulsators have a dominant overtone mode, with many sources pulsating in the second overtone or higher order modes. The fundamental mode pulsators have metallicity-dependent periods, with $\log_{10}(P) \sim -1.1$ for [Fe/H] < -0.3 and $\log_{10}(P) \sim -0.9$ for [Fe/H] > 0, which leads to a period-dependent scale height. Stars with $P > 0.100$ d are predominantly located close to the Galactic disc ($|Z| < 0.5$ kpc). The median period at a scale height of $Z \sim 0$ kpc also increases with the Galactocentric radius R, from $\log_{10}(P) \sim -0.94$ for sources with $R > 9$ kpc to $\log_{10}(P) \sim -0.85$ for sources with $R < 7$ kpc, which is indicative of a radial metallicity gradient. To illustrate potential applications of this all-sky catalogue, we obtained 30 min cadence, image subtraction *TESS* light curves for a sample of 10 fundamental mode and 10 overtone δ Scuti stars discovered by ASAS-SN. From this sample, we identified two new δ Scuti eclipsing binaries, ASASSN-V J071855.62−434247.3 and ASASSN-V J170344.20−615941.2 with short orbital periods of $P_{\rm orb} = 2.6096$ and 2.5347 d, respectively.

Key words: stars: binaries: eclipsing – stars: variables: Delta Scuti – stars: variables – catalogues – surveys.

1 INTRODUCTION

δ Scuti stars are intermediate-mass variable stars with spectral types between A2 and F2 that pulsate at high frequencies (0.02 d $< P <$ 0.25 d) with typical amplitudes in the V band of 3 mmag $< A <$ 0.9 mag (Chang et al. 2013; Bowman 2017). They have temperatures in the range 6900 K $< T_{\rm eff} <$ 8900 K while on the zero-age main sequence (ZAMS) and are located where the classical instability strip intersects the ZAMS (Breger 1979; Rodríguez & Breger 2001). δ Scuti stars have masses in the range 1.5 $M_\odot < M <$ 2.5 $M_\odot$, which places them in the transition regime between low-mass stars having convective envelopes and high-mass stars having radiative envelopes and convective cores (Bowman 2017). Thus, the pulsations in δ Scuti stars allow for detailed studies of stellar structure and evolution in this transition regime (Bowman & Kurtz 2018). Most δ Scuti stars tend to cross the instability strip on approximately horizontal tracks, placing them in the core hydrogen

★ E-mail: jayasinghearachchilage.1@osu.edu

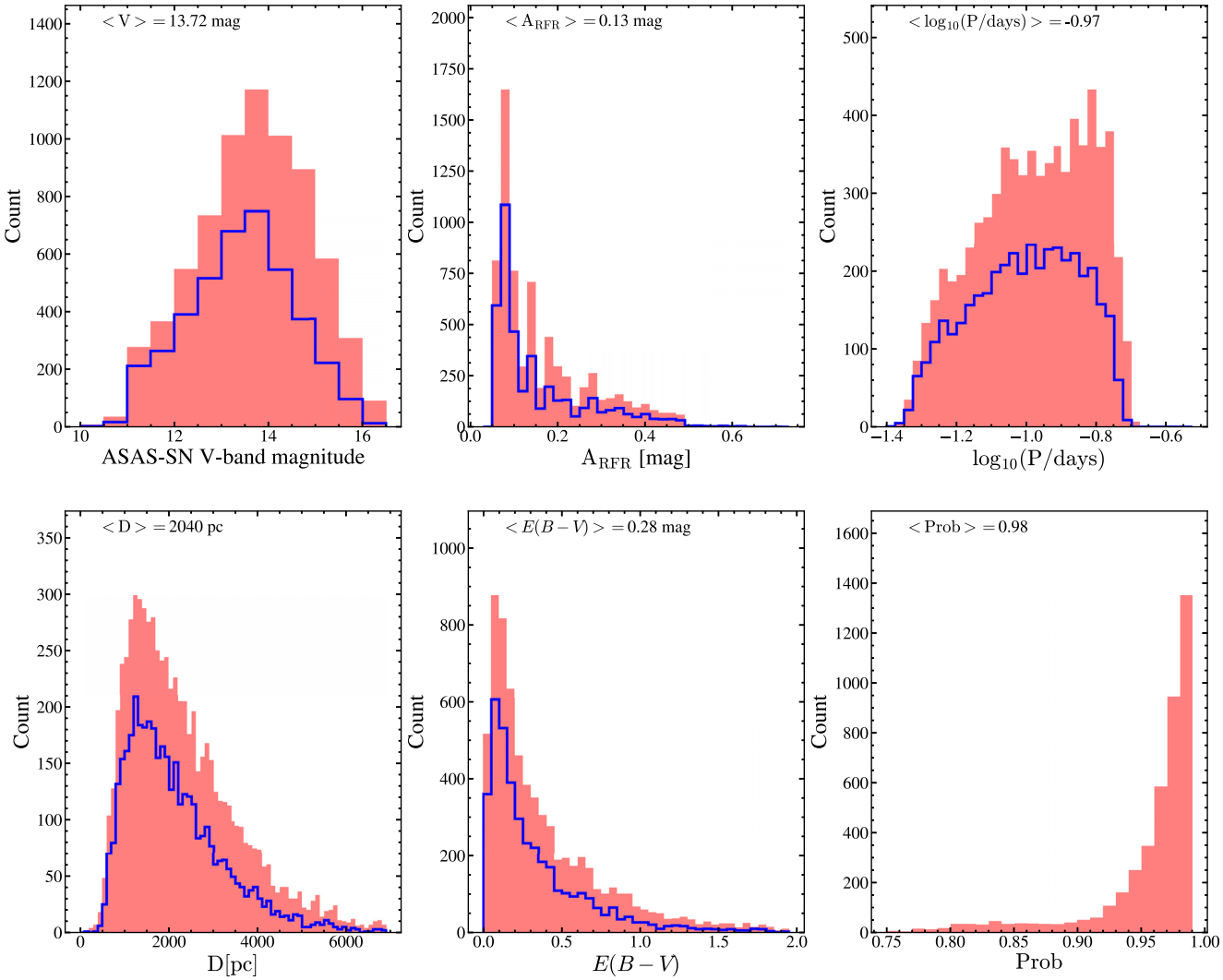

Figure 1. Distribution of the ASAS-SN δ Scuti stars in their V-band magnitude, amplitude ($A_{\rm RFR}$), period, distance, reddening, and classification probability. The median value for each feature is listed. The blue histograms show the distribution of δ Scuti stars with classification probabilities greater than the median classification probability for the entire sample (Prob > 0.98).

burning or early hydrogen shell burning evolutionary stages (Breger 2000; Aerts, Christensen-Dalsgaard & Kurtz 2010).

Most δ Scuti stars are multiperiodic pulsators, with both high-amplitude radial pulsations and low-amplitude non-radial pulsations (Bowman 2017). These pulsations are driven by the κ mechanism in the He II partial ionization zone (Breger 2000; Aerts et al. 2010). The κ mechanism can produce pressure (p) modes with periods between 15 min and 8 h (Uytterhoeven et al. 2011; Holdsworth et al. 2014). Recently, studies of *Kepler* light curves found that ∼25 per cent of the δ Scuti stars were in fact hybrid pulsators, having both p modes excited by the κ mechanism and gravity (g) modes excited by the convective flux blocking mechanism (Balona & Dziembowski 2011; Uytterhoeven et al. 2011; Bowman & Kurtz 2018). The rich range of pulsation modes in δ Scuti stars has been studied extensively using both ground-based and space-based observatories (Breger et al. 1998, 1999; Breger 2000; Bowman & Kurtz 2018; Guzik, Garcia & Jackiewicz 2019).

Much like RR Lyrae stars and Cepheids that also pulsate due to the κ mechanism, δ Scuti stars are known to follow a period–luminosity relationship (PLR; Breger & Bregman 1975; McNamara 1997; Poleski et al. 2010; Ziaali et al. 2019). The scatter in the δ Scuti PLR tends to be somewhat larger than that observed in the PLRs of RR Lyrae and Cepheids. δ Scuti stars can pulsate in the fundamental mode ($n = 1$) and overtone modes ($n = 2, 3, 4, ...$). These modes are either radial ($l = 0$) or non-radial ($l = 1, 2, 3, 4, ...$) (Ziaali et al. 2019). In general, the most likely pulsation mode observed in the δ Scuti PLR is the radial fundamental mode ($n = 1$, $l = 0$).

The All-Sky Automated Survey for SuperNovae (ASAS-SN; Shappee et al. 2014; Kochanek et al. 2017), using two units in Chile and Hawaii each with 4 telescopes, monitored the visible sky to a depth of $V \lesssim 17$ mag with a cadence of 2–3 d. ASAS-SN has since expanded to 5 units with 20 telescopes and is currently monitoring the sky in the g band to a depth of $g \lesssim 18.5$ mag with a cadence of ∼1 d. The ASAS-SN telescopes are hosted by the Las Cumbres Observatory (LCO; Brown et al. 2013) in Hawaii, Chile, Texas, and South Africa. ASAS-SN is well suited for the characterization of stellar variability across the whole sky due to its excellent baseline and all-sky coverage.

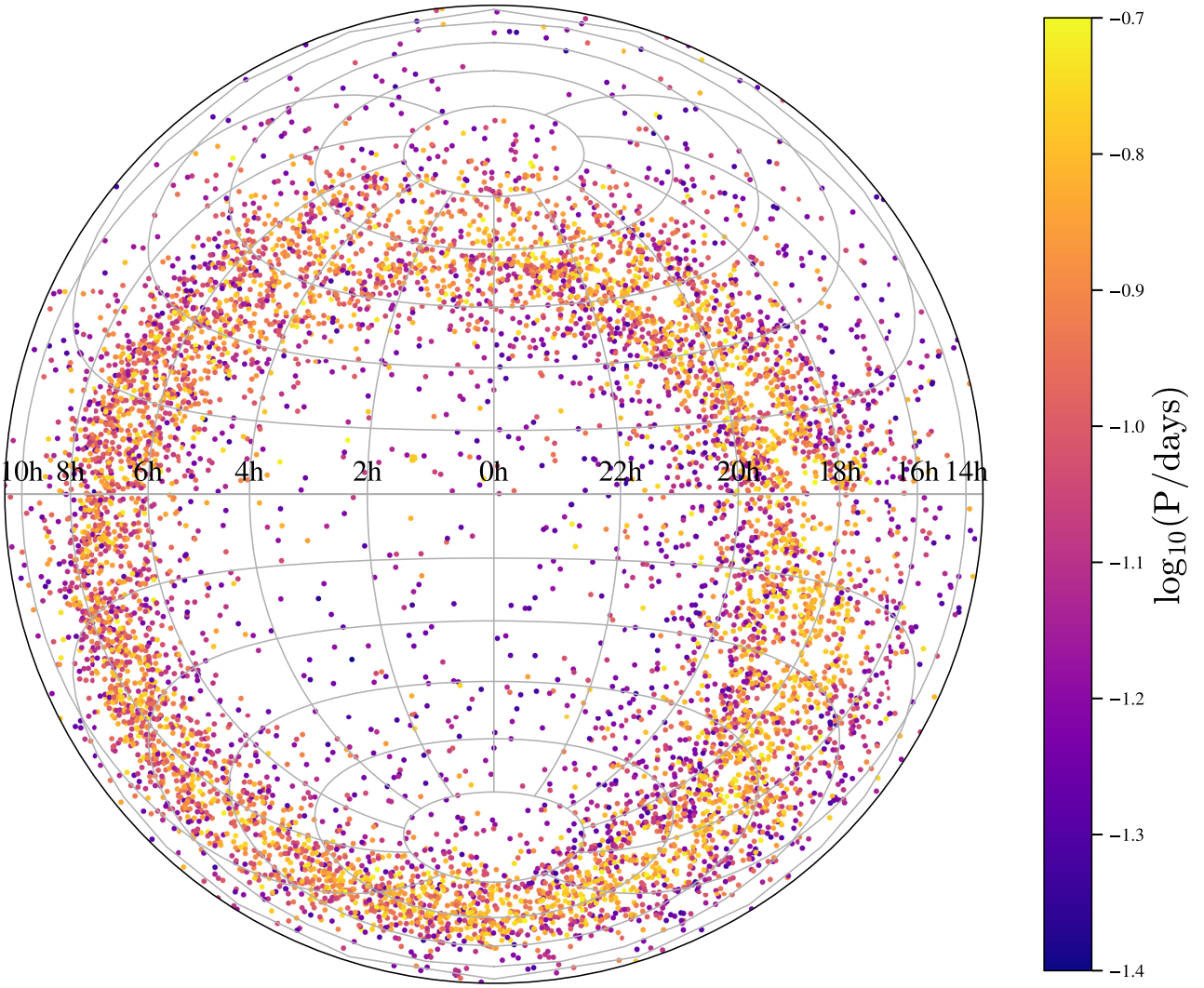

Figure 2. Spatial distribution of the ∼8400 δ Scuti stars in Equatorial coordinates (Lambert projection). The points are coloured by period. Note how the longer period stars tend to be closer to the Galactic plane.

In a series of papers (Jayasinghe et al. 2018, 2019b, d), we have been systematically identifying and classifying variables from the ASAS-SN *V*-band data. This includes discovering ∼220 000 new variables and homogeneously classifying both the new and previously known variables in this magnitude range (Jayasinghe et al. 2019a). We are also exploring the synergies between ASAS-SN and large-scale spectroscopic surveys starting with APOGEE (Holtzman et al. 2015; Thompson et al. 2018; Pawlak et al. 2019).

Here, we analyse an all-sky catalogue of 8418 δ Scuti stars in the ASAS-SN *V*-band data. In Section 2, we summarize the ASAS-SN catalogue of δ Scuti stars and the cross-matching to external photometric and spectroscopic catalogues. We derive PLRs in Section 3 and analyse the sample of δ Scuti stars with spectroscopic cross-matches in Section 4. We present an analysis of 20 δ Scuti stars discovered by ASAS-SN using Transiting Exoplanet Survey Satellite (*TESS*) light curves in Section 5 and summarize our work in Section 6. The *V*-band light curves and other variability and photometric information for all of the ∼8400 sources studied in this work are available online at the ASAS-SN variable stars data base (https://asas-sn.osu.edu/variables).

2 THE ASAS-SN CATALOGUE OF δ SCUTI STARS

In this work, we selected 8418 δ Scuti stars identified during our systematic search for variables. This includes new δ Scuti stars in the Northern hemisphere (Jayasinghe et al. 2020, in prep.) and regions of the southern Galactic plane that were missed in the previous survey papers (Jayasinghe et al. 2019d). Out of the 8418 δ Scuti stars in this catalogue, 3322 (∼40 per cent) are new ASAS-SN discoveries. The ASAS-SN *V*-band observations used in this work were made by the 'Brutus' (Haleakala, Hawaii) and 'Cassius' (CTIO, Chile) quadruple telescopes between 2013 and 2018. Each ASAS-SN *V*-band field is observed to a depth of $V \lesssim 17$ mag. The field of view of an ASAS-SN camera is 4.5 deg^2, the pixel scale is 8.″0, and the full width at half-maximum is typically ∼2 pixels. ASAS-SN tends to saturate at ∼10−11 mag, but we attempt to correct the light curves of saturated sources for bleed trails (see Kochanek et al. 2017). The *V*-band light curves were extracted as described in Jayasinghe et al. (2018) using image subtraction (Alard & Lupton 1998; Alard 2000) and aperture photometry on the subtracted images with a 2 pixel radius aperture. The APASS

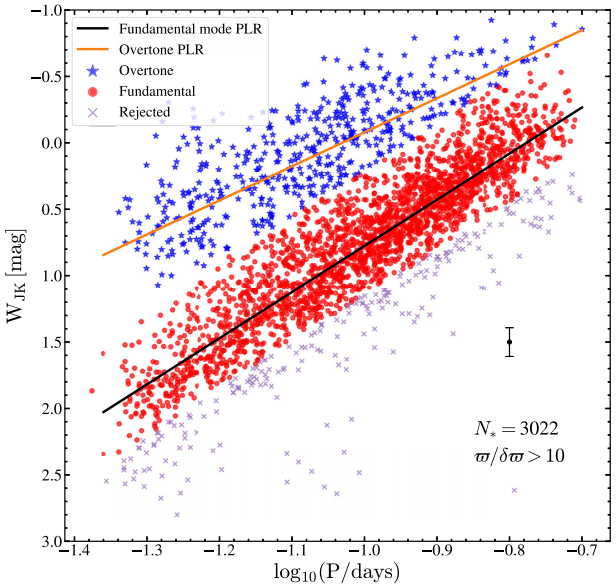

Figure 3. The Wesenheit W_{JK} PLR diagram for the δ Scuti stars with Prob > 0.98 (fundamental mode) and Prob > 0.90 (overtone) and parallaxes better than 10 per cent. The fitted PLRs for the fundamental mode and overtone pulsators are shown as black and orange lines, respectively. The average uncertainties are shown in black.

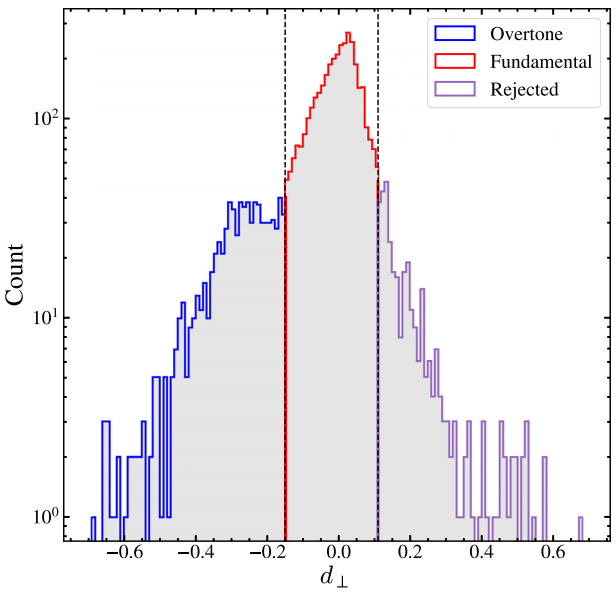

Figure 4. Distribution of the perpendicular distances to an initial fundamental mode Wesenheit W_{JK} PLR fit. The distributions of the fundamental mode pulsators (red), likely overtone pulsators (blue), and rejected candidates (purple) are shown as histograms. The shaded grey histogram is for the entire sample.

catalogue (Henden et al. 2015) and the ATLAS All-Sky Stellar Reference Catalog (Tonry et al. 2018) were used for calibration. We corrected the zero-point offsets between the different cameras as described in Jayasinghe et al. (2018). The photometric errors were recalculated as described in Jayasinghe et al. (2019b). Variable sources were identified and subsequently classified using two independent random forest classifiers and quality checks as described in Jayasinghe et al. (2019a, d). We used the `astropy` implementation

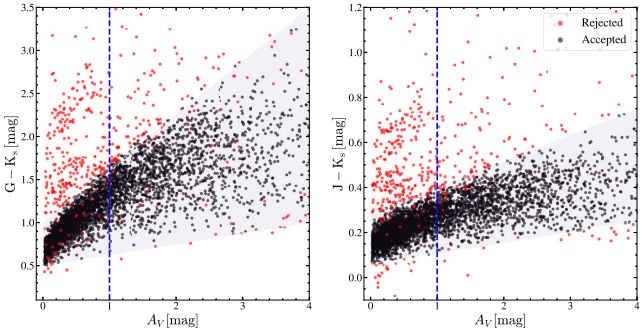

Figure 5. Distribution of the δ Scuti stars in the $G - K_s$ (left) and $J - K_s$ (right) colour-extinction spaces. Sources inside (outside) the shaded region and coloured in black (red) are defined to have acceptable (bad) colours and/or extinctions. The sources with bad colours and/or extinctions deviate from the expected distribution of the δ Scuti stars in the $G - K_s$ and $J - K_s$ colour-extinction spaces and are not considered in our work. The curvature towards higher A_V enters as the distinction between the total Galactic extinction and the actual extinction to the star becomes important.

of the generalized Lomb–Scargle (Scargle 1982; Zechmeister & Kürster 2009) periodogram to search for periodicity over the range $0.05 \leq P \leq 1000$ d for these δ Scuti stars.

We cross-matched the δ Scuti stars with *Gaia* DR2 (Gaia Collaboration 2018a) using a matching radius of 5.″0. The sources were assigned distance estimates from the *Gaia* DR2 probabilistic distance estimates (Bailer-Jones et al. 2018) by cross-matching based on the *Gaia* DR2 `source_id`. We also cross-matched these sources to the 2MASS (Skrutskie et al. 2006) and AllWISE (Wright et al. 2010; Cutri et al. 2013) catalogues using a matching radius of 10.″0. We used `TOPCAT` (Taylor 2005) for this process. Following the cross-matching process, we calculated the absolute, reddening-free Wesenheit magnitude (Madore 1982; Lebzelter et al. 2018) for each source as

$$W_{JK} = M_{K_s} - 0.686(J - K_s)\,. \quad (1)$$

For each source, we also calculate the total line-of-sight Galactic reddening $E(B - V)$ from the recalibrated 'SFD' dust maps (Schlegel, Finkbeiner & Davis 1998; Schlafly & Finkbeiner 2011) using `dustmaps` (Green 2018).

To explore the synergy between ASAS-SN and large spectroscopic surveys, we also cross-matched the variables with the APOGEE DR15 catalogue (Holtzman et al. 2015; Majewski et al. 2017), the RAVE-on catalogue (Casey et al. 2017), the LAMOST DR5 v4 catalogue (Cui et al. 2012), and the GALAH DR2 catalogue (De Silva et al. 2015; Buder et al. 2018) using a matching radius of 5.″0. We identified 972 matches to the δ Scuti stars, with all the cross-matches coming from the LAMOST (86.7 per cent), GALAH (10.0 per cent), or RAVE (3.2 per cent) surveys. The LAMOST DR5 v4 catalogue also lists the spectral type of each source, and the majority of the cross-matches from LAMOST have a spectral type of F0 (55.6 per cent), A7V (20.1 per cent), or A6IV (5.0 per cent).

We illustrate the distribution of the ASAS-SN δ Scuti stars in their V-band magnitude, amplitude ($A_{\rm RFR}$), period, distance, reddening, and classification probability in Fig. 1. The variability amplitude $A_{\rm RFR}$ is calculated using a non-parametric random forest regression model (Jayasinghe et al. 2019a). The majority of the sources are brighter than $V = 16$ mag, as ASAS-SN loses sensitivity to low-amplitude variability at fainter magnitudes. The distribution of the

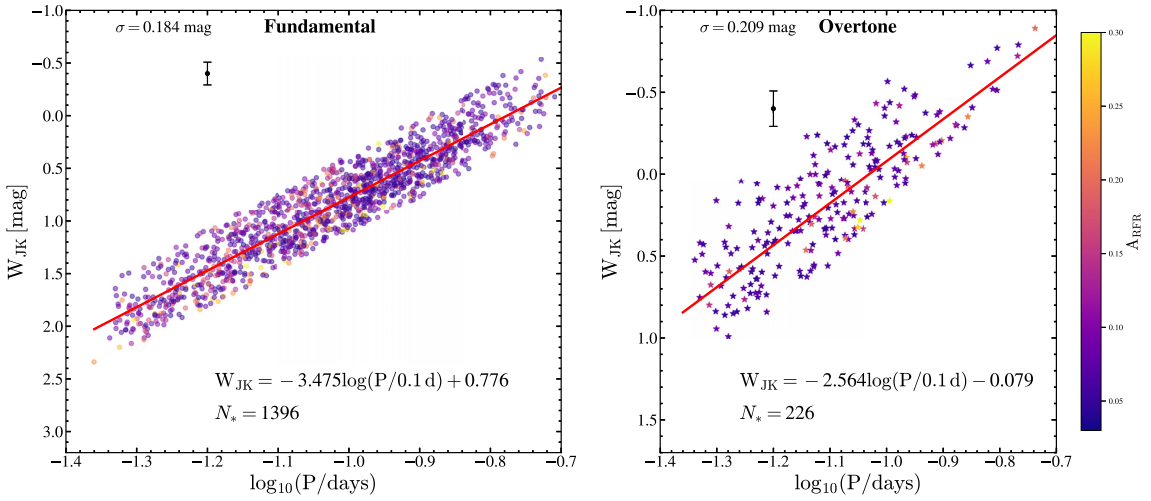

Figure 6. The Wesenheit W_{JK} PLR for the fundamental mode (left) and overtone (right) δ Scuti stars. The fitted PLR is shown in red and the points are coloured by the variability amplitude $A_{\rm RFR}$.

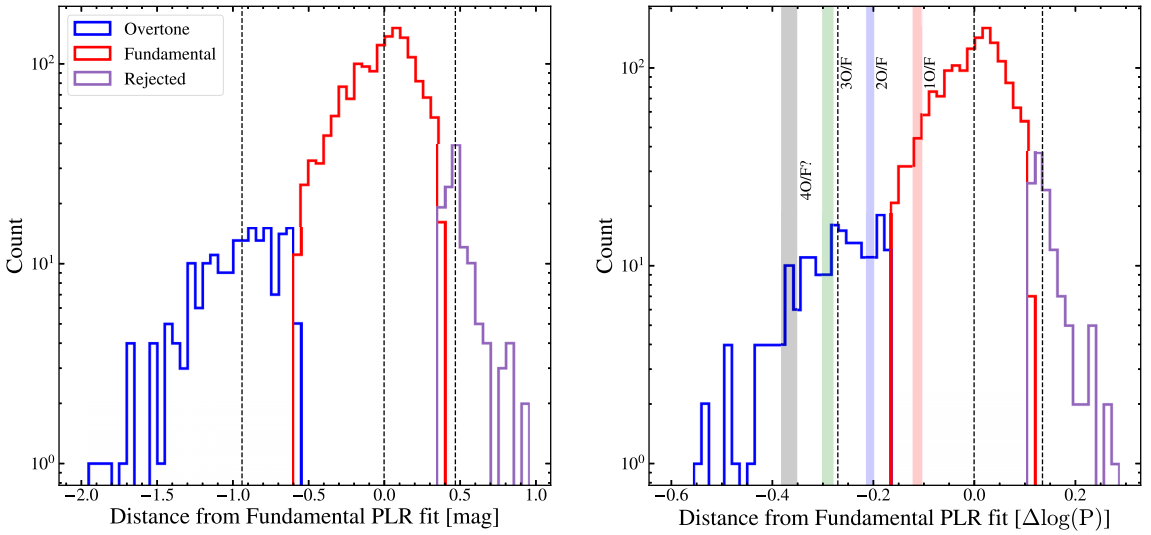

Figure 7. Distribution of the δ Scuti stars in the vertical (ΔW_{JK}, left) and horizontal ($\Delta \log_{10} P$, right) deviations from the fundamental mode PLR fit. The dashed black lines show the median value of the deviations. The range of expected period ratios for δ Scuti stars pulsating in the first overtone (red), the second overtone (blue), or the third overtone (green) is shaded (Stellingwerf 1979). The likely range of period ratios for the fourth overtone is shaded in black.

Table 1. PLR parameters for the fundamental mode δ Scuti.

Band	A mag	B mag	σ mag
W_{JK}	-3.475 ± 0.034	0.776 ± 0.004	0.184
V	-3.006 ± 0.479	1.493 ± 0.245	0.227
G	-3.047 ± 0.555	1.532 ± 0.301	0.210
J	-3.330 ± 0.064	0.997 ± 0.079	0.188
H	-3.373 ± 0.037	0.894 ± 0.060	0.185
K_s	-3.397 ± 0.044	0.868 ± 0.064	0.183
W_1	-3.385 ± 0.036	0.834 ± 0.036	0.190

Table 2. PLR parameters for the overtone δ Scuti.

Band	A mag	B mag	σ mag
W_{JK}	-2.564 ± 0.138	-0.079 ± 0.013	0.209
V	-1.980 ± 0.144	0.613 ± 0.019	0.291
G	-1.969 ± 0.128	0.659 ± 0.018	0.263
J	-2.045 ± 0.121	0.170 ± 0.013	0.223
H	-2.299 ± 0.147	0.053 ± 0.016	0.213
K_s	-2.439 ± 0.139	0.021 ± 0.015	0.209
W_1	-2.560 ± 0.142	-0.032 ± 0.070	0.218

δ Scuti stars in amplitude is as expected, with the vast majority having amplitudes $A_{\rm RFR} < 0.30$ mag. Classification probabilities of Prob > 0.9 are very reliable and ∼92 per cent of our sample of δ Scuti stars have Prob > 0.9 and the median classification probability is Prob $= 0.98$. The distribution of these sources in period has a sharp cut-off around $P \sim 0.2$ d [$\log_{10}(P/\text{days}) \sim -0.7$]. This is an artificial cut-off implemented in our classification pipeline to minimize contamination from short-period RR Lyrae and contact binary stars. The distribution of periods appears to show an excess of sources around $\log_{10}(P/\text{days}) \sim -0.8$, but this excess is not seen

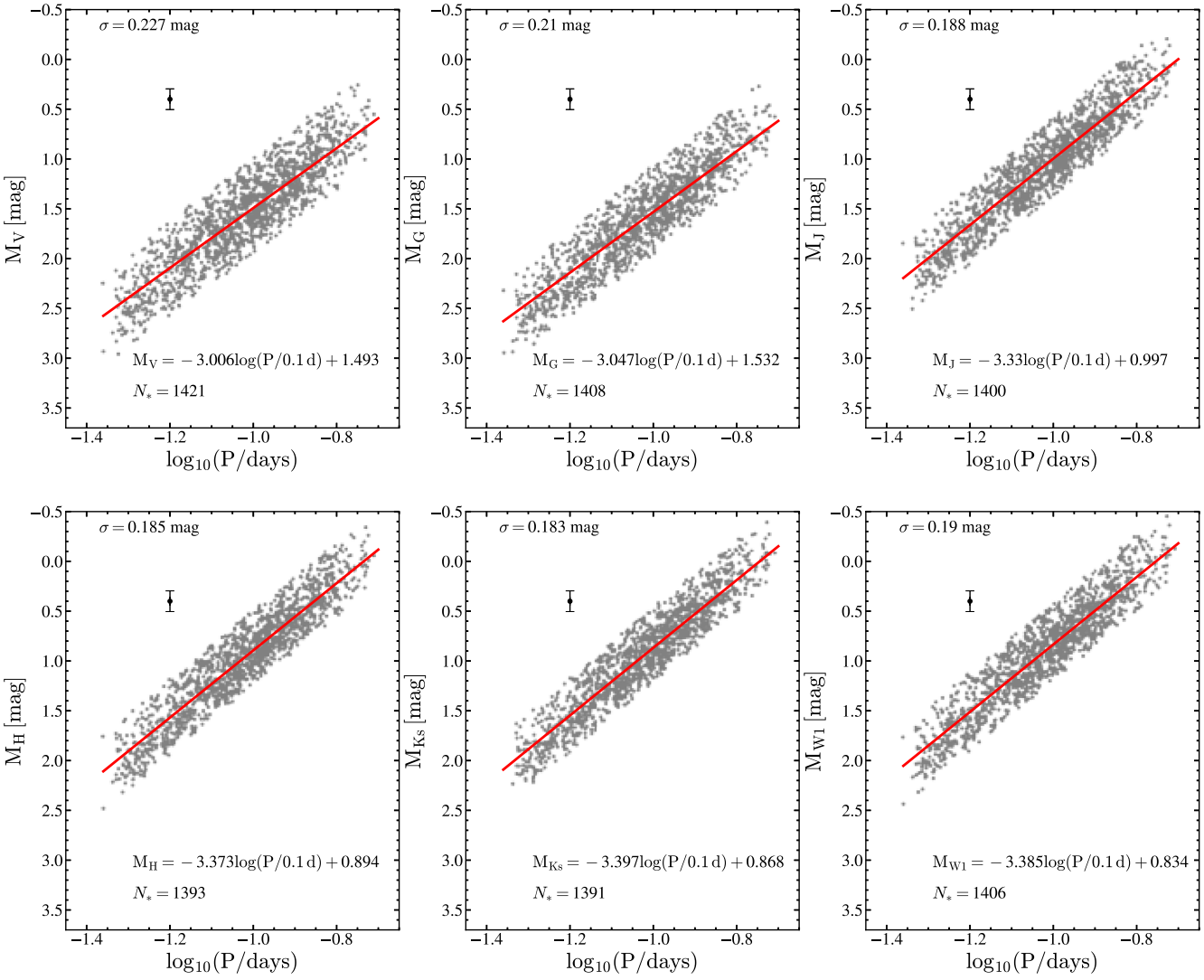

Figure 8. The PLRs for the fundamental mode δ Scuti stars in the V, *Gaia* DR2 G, J, H, K_s, and W_1 bands. The average uncertainty in M_λ is shown in black. The fitted PLR is shown in red.

in the distribution of periods for the subset of sources with Prob > 0.98, possibly indicating some contamination from other variable groups.

There are 746 sources within 1 kpc but most (∼91 per cent) of the sources are located further away. A large fraction have useful parallaxes, as ∼79 per cent (∼63 per cent) of the sources have `parallax/parallax_error` >5 (>10). The median value of the reddening $E(B-V)$ indicates substantial extinction ($A_V \sim 0.87$ mag), assuming $R_V = 3.1$ dust (Cardelli, Clayton & Mathis 1989). This is not too surprising as these stars tend to be located towards the Galactic disc with 75 per cent of the δ Scuti stars within $|b| < 18.4$ deg. The sky distribution of the δ Scuti stars in ASAS-SN, coloured by their period, is shown in Fig. 2. There is a clear gradient of increasing period towards lower Galactic latitudes, which suggests a metallicity dependence to the period of these stars. We will explore this dependence further in Section 4.

High-amplitude δ Scuti (HADS) stars are a subset of the δ Scuti class that pulsate in radial modes with large amplitudes (McNamara 2000). The classification scheme that is used by ASAS-SN follows the definitions of the VSX catalogue (Watson, Henden & Price 2006), which defines HADS stars as those with V-band amplitudes $A > 0.15$ mag. However, canonically, HADS stars have been defined with an amplitude cut-off of $A > 0.30$ mag. With the VSX definition, our catalogue contained 3989 HADS sources, of which 3660 (2086) have Prob > 0.9 (Prob > 0.98). With the canonical definition, our catalogue contained 1496 HADS sources, of which 1406 (865) have Prob > 0.9 (Prob > 0.98).

3 PERIOD-LUMINOSITY RELATIONSHIPS

Fig. 3 shows the Wesenheit W_{JK} PLR diagram for the δ Scuti stars. We identify two possible PLRs corresponding to the fundamental and overtone modes of pulsation (Fig. 4). Previous studies have derived PLRs for the δ Scuti stars using a smaller number of sources (McNamara 2011; Ziaali et al. 2019). In addition, similar PLR sequences have been previously studied for other classes of pulsating variables including RR Lyrae and Cepheids (see, for e.g., the review by Beaton et al. 2018).

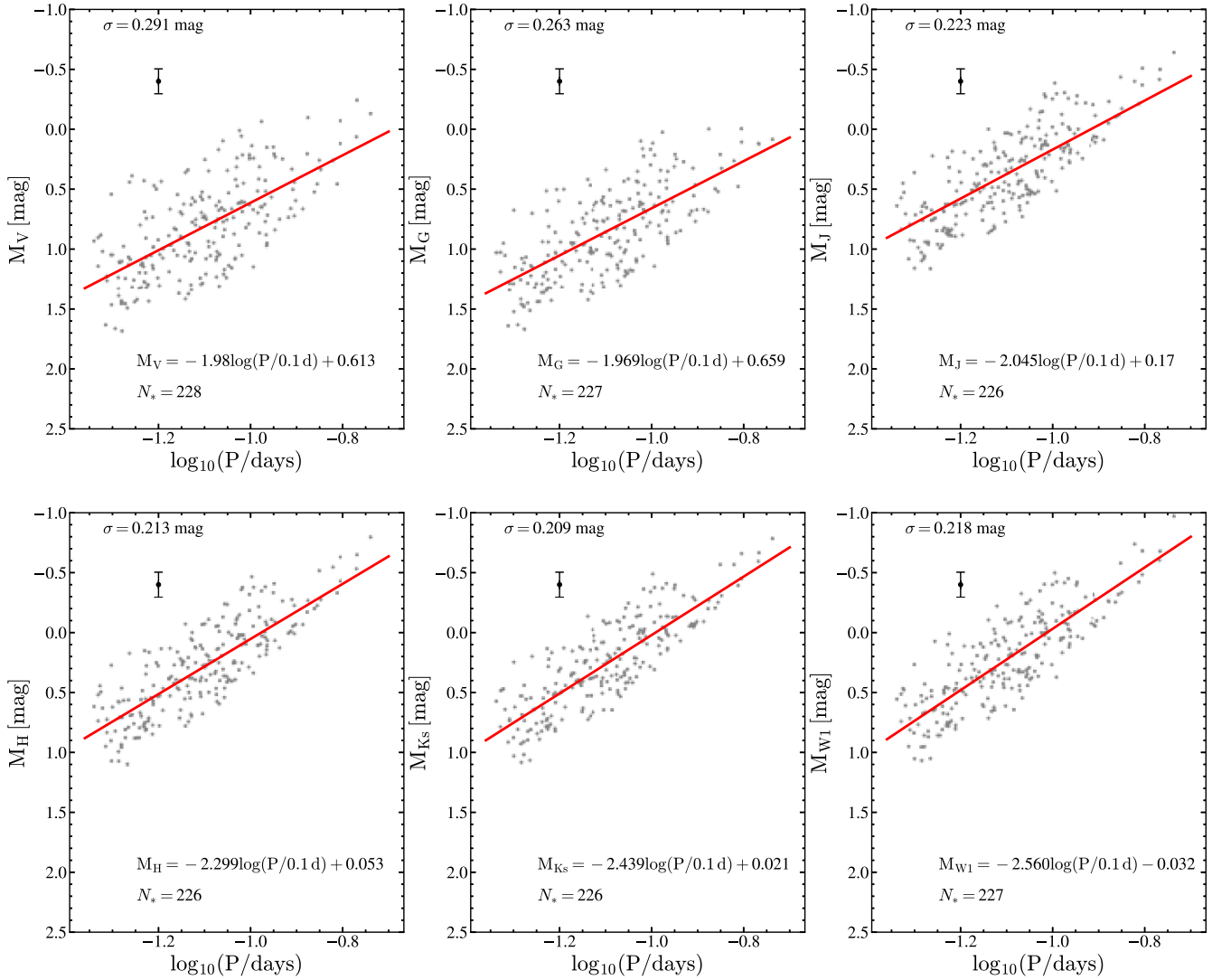

Figure 9. The PLRs for the overtone δ Scuti stars in the V, *Gaia* DR2 G, J, H, K_s, and W_1 bands. The average uncertainty in M_λ is shown in black. The fitted PLR is shown in red.

We sorted the sample of sources into three categories consisting of fundamental mode pulsators, likely overtone pulsators, and rejected candidates. Initially, we empirically selected a sample of ∼1500 fundamental mode pulsators from our catalogue and fit a PLR with the form

$$W_{JK} = -3.495 \log_{10}(P/0.1\,\mathrm{d}) + 0.767.$$

Next, we calculated the perpendicular distances ($d_\perp$) from this initial PLR for each source in our catalogue (Fig. 4). Based on the distribution of these distances, we separate the δ Scuti stars into fundamental mode sources ($-0.15 \leq d_\perp \leq 0.11$), overtone sources ($d_\perp < -0.15$), and rejected candidates ($d_\perp > 0.11$). These cuts were motivated by the drop in the distribution centred at $d_\perp \sim 0$, corresponding to the fundamental mode pulsators. Fig. 3 shows the Wesenheit W_{JK} PLR diagram for these sources, with the fitted PLRs shown. The set of rejected candidates is located to the right of the fundamental mode PLR sequence and likely consists of γ Dor stars with harmonics above 5 d^{-1} (Murphy et al. 2019; Ziaali et al. 2019). Given that the overtone pulsators are rare and that the training set was biased by the large number of fundamental mode pulsators, we expect δ Scuti stars pulsating in a dominant overtone mode to have somewhat lower classification probabilities in our pipeline. Thus, we choose two different cut-offs in classification probability to improve the quality of our PLRs. When constructing PLRs, we choose fundamental mode pulsators with Prob > 0.98, which corresponds to the mean classification probability of our entire sample. For the overtone pulsators, we relax this cut-off to Prob > 0.9, which still implies a robust classification. We also implement a cut-off of `parallax/parallax_error` >10 to reduce the uncertainty in the absolute magnitudes.

The SFD reddening estimates are totals for the line of sight rather than for stars at a particular distance. Fig. 5 shows the $G - K_s$ and $J - K_s$ colours of the stars as a function of A_V. These finite distance effects manifest as a curvature in the colour distribution for larger A_V. To minimize this problem, we use a limit of $A_V < 1$ mag for stars used to construct the PLRs. We also see a scattering of stars with inconsistent colours/extinctions, and we eliminate these stars as well.

For the non-Wesenheit PLRs, we corrected for the interstellar extinction using the SFD estimate of the reddening, the relative extinction coefficients $A_G/A_V = 0.859\ 26$, $A_J/A_V = 0.294\ 34$,

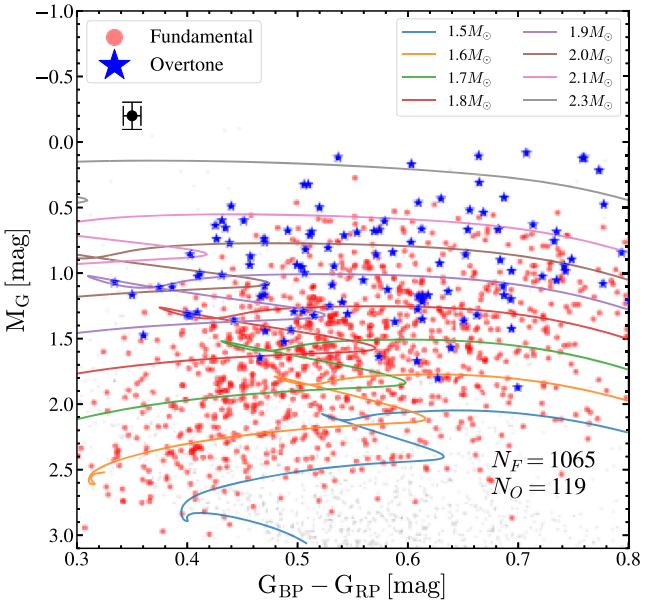

Figure 10. *Gaia* DR2 colour–magnitude diagram for a sample of the fundamental mode and overtone pulsators with $A_V < 0.5$ mag and parallaxes better than 10 per cent. A sample of nearby sources with good parallaxes and photometry is shown in grey. Solar metallicity stellar evolution tracks from MIST (Choi et al. 2016; Dotter 2016) are shown for comparison. The average uncertainties are shown in black.

$A_H/A_V = 0.181\,28$, $A_{K_s}/A_V = 0.118\,38$, $A_{W1}/A_V = 0.071\,34$, and

$$M_\lambda = m_\lambda - 5\log(d) + 5 - A_\lambda, \quad (2)$$

where d is the *Gaia* DR2 probabilistic distance estimate (Bailer-Jones et al. 2018). We then fit PLRs of the form

$$M_\lambda = A\log_{10}(P/0.1\,\mathrm{d}) + B, \quad (3)$$

using the Levenberg– Marquardt chi-square minimization routine in `scikit-learn` (Pedregosa et al. 2012). After the initial fit, we removed outliers from the PLR fit for each band by calculating the distance from an initial fit

$$r = \sqrt{(\Delta\log_{10} P)^2 + (\Delta M_\lambda)^2},$$

where

$$\Delta\log_{10}(P) = \log_{10}(P_{\rm fit}/P_{\rm obs})$$

and

$$\Delta M_\lambda = M_{\lambda,\rm fit} - M_{\lambda,\rm obs}.$$

Sources that deviated from this fit by $>3\sigma_r$ were removed. After removing these outliers, the parameters from the trial fit were then used to initialize a Monte Carlo Markov Chain sampler (MCMC) with 200 walkers, which were run for 20 000 iterations. We used the MCMC implementation `emcee` (Foreman-Mackey et al. 2013). The errors in the PLR parameters were derived from the MCMC chains.

We fit Wesenheit W_{JK} magnitude PLRs to both the fundamental mode and overtone sample as shown in Fig. 6. The variability amplitudes of the overtone pulsators tend to be smaller than those of fundamental mode pulsators. The overtone sample likely encompasses sources with different dominant overtones, so the PLR fit is to an average distribution, and not a particular overtone. We also looked at the deviation from the PLR fit in the horizontal [$\Delta(\log_{10}(P))$] and vertical (ΔW_{JK}) directions (Fig. 7). Expected period ratios for combinations of the fundamental mode and the first three overtone modes are highlighted (Stellingwerf 1979). It is clear that the distributions of these sources in $\Delta(\log_{10}P)$ and ΔW_{JK} follow a bimodal distribution, with the overtone sources clearly distinct from the fundamental mode pulsators. The overtone sources have median displacements from the fundamental mode PLR fit of $\Delta\log_{10}P \sim -0.27$ and $\Delta W_{JK} \sim -0.94$. The vertical displacement is reminiscent of overtone populations in other classical pulsators (for e.g. Beaulieu et al. 1995 noted that overtone Cepheids formed a PLR sequence ∼1 mag brighter than the fundamental PLR for Cepheid variables). Ziaali et al. (2019) noted an excess of sources in a ridge to the left of the fundamental ridge and found a similar displacement in $\Delta\log_{10}P$. This value of $\Delta\log_{10}P$ corresponds to a period ratio with the fundamental mode of $P/P_{\rm F} \sim 0.535$, which is consistent with the period ratios expected for the third overtone from theoretical models of δ Scuti stars (Stellingwerf 1979). Indeed, Ziaali et al. (2019) suggested the possibility of a resonant third or fourth overtone mode of pulsation as the mechanism behind the additional PLR sequence. We also note an additional peak at $\Delta\log_{10}P \sim -0.37$, which corresponds to a period ratio with the fundamental mode of $P_{\rm O}/P_{\rm F} \sim 0.43$. We suspect that this could be the fourth overtone but we were unable to find any theoretical predictions of period ratios for the fourth overtone.

Next, after correcting for interstellar extinction with the SFD estimate, we perform PLR fits in the V, *Gaia* DR2 G, J, H, K_s, and W_1 bands for both the fundamental mode and overtone pulsators. The best-fitting parameters, their uncertainties, and the standard deviation from the PLR fit (σ) are listed in Table 1 (fundamental) and Table 2 (overtone). We have illustrated these fits in Fig. 8 (fundamental) and Fig. 9 (overtone). The PLR derived in the V band is consistent within uncertainties to those obtained by previous studies (McNamara 2011; Ziaali et al. 2019). The PLRs for the overtone pulsators have a larger scatter and uncertainty when compared to the corresponding fundamental mode PLRs. This is in part due to the relative rarity of the overtone pulsators when compared to the fundamental mode pulsators. In addition, the overtone sample likely encompasses sources with different dominant overtones, so the PLR fit is to an average distribution, and not that of a particular overtone. As is typical of PLRs, the near-infrared PLRs have smaller uncertainties and scatter than the PLRs in the optical. This effect is more pronounced for the overtone sources than for the fundamental mode pulsators.

Fig. 10 shows the positions of a sample of the fundamental mode and overtone pulsators with $A_V < 1$ mag and parallaxes better than 10 per cent in a *Gaia* DR2 colour–magnitude diagram (CMD) after correcting for interstellar extinction. A sample of nearby sources with good parallaxes and photometry is shown in the background. To compare the observational data with theoretical models, we also show the MESA Isochrones and Stellar Tracks (MIST) stellar evolution models (Choi et al. 2016; Dotter 2016) for stars with masses of 1.5, 1.6, 1.7, 1.8, 1.9, 2.0, 2.1, and 2.3 $M_\odot$ starting from the ZAMS. We assumed Solar metallicity and no extinction for these models. The overtone pulsators largely have $M_G > 2$ mag and appear to be consistent with the stellar evolution tracks with masses $1.8\,M_\odot < M < 2.1\,M_\odot$. In contrast, the fundamental mode pulsators appear to span a wider range of masses and luminosities that overlap with the overtone pulsators.

We investigate how the fundamental mode W_{JK} PLR varies with pulsational amplitude and the *Gaia* DR2 distances. We studied the variation of the PLR fits in amplitude bins with $A_{\rm RFR} < 0.15$ mag, 0.15 mag $< A_{\rm RFR} < 0.30$ mag, and $A_{\rm RFR} > 0.30$ mag and found that

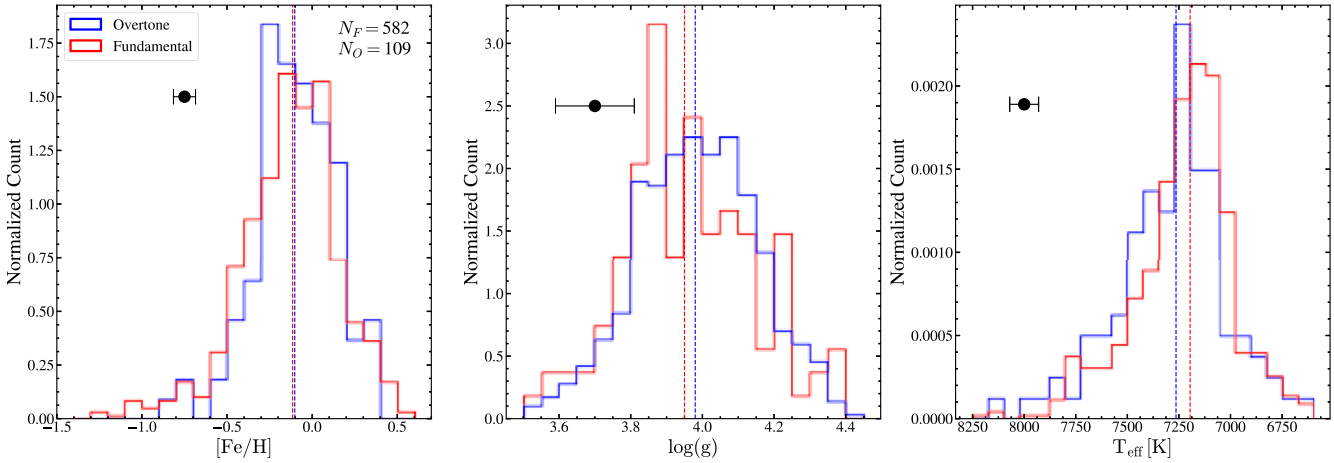

Figure 11. Distributions of the fundamental mode (red) and overtone (blue) δ Scuti stars in [Fe/H], log(g), and $T_{\rm eff}$. The median value for each parameter is illustrated with a dashed line. The average uncertainty for each parameter is shown in black.

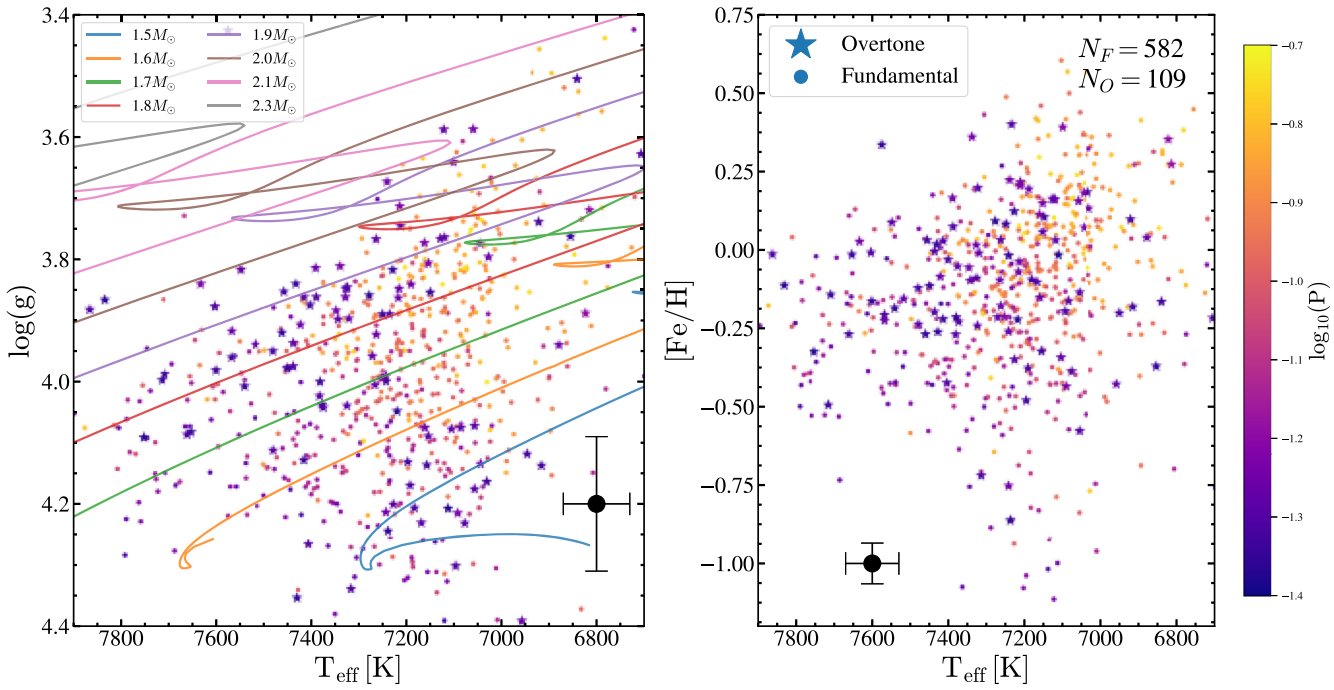

Figure 12. Distributions of the fundamental mode and overtone δ Scuti stars in log(g) versus $T_{\rm eff}$ (left) and $T_{\rm eff}$ versus [Fe/H] (right). The points are coloured by the pulsational period. Solar metallicity stellar evolution tracks from MIST (Choi et al. 2016; Dotter 2016) are shown for comparison. The average uncertainties are shown in black.

the W_{JK} PLR fits remained consistent with the overall fit (Table 1). We also investigated the variation of the PLR fits in distance bins with $D < 1$ kpc, 1 kpc $< D < 2$ kpc, and $D > 2$ kpc. The W_{JK} PLR fits remain consistent with the overall fit in the bins $D < 1$ kpc and 1 kpc $< D < 2$ kpc, but the PLR fit for the bin $D > 2$ kpc differs slightly from the overall fit. This is likely due to the decreasing reliability of *Gaia* DR2 distances at scales larger than $\sim$1$-$2 kpc, which introduces additional vertical scatter in the PLR.

In addition, Murphy et al. (2019) noted that the $\sim$29 μas global zero-point parallax offset implemented in the distance estimates by Bailer-Jones et al. (2018) resulted in underestimated luminosities for A-type stars. To investigate the effects of this parallax offset on the PLRs, we recalculated the PLRs by selecting sources with `parallax/parallax_error` >20 where the effect of a parallax offset should be minimal. For these sources, this offset corresponds to roughly $\sim$1$\times$ the parallax uncertainties. We find that the parameters of the PLR fits change by < 2 per cent. Since the PLR fits are not dramatically different, the impact of the zero-point parallax offset on the PLRs should be negligible.

4 THE SPECTROSCOPIC SUB-SAMPLE

We found 972 cross-matches to LAMOST, GALAH, or RAVE. Fig. 11 shows the distributions in effective temperature $T_{\rm eff}$, surface gravity log(g), and metallicity [Fe/H] for both the fundamental mode and overtone δ Scuti. Given the relatively small number of sources with spectroscopic data, we relax the cut-offs implemented in Section 3.1 and consider sources with Prob > 0.9, and `paral-`

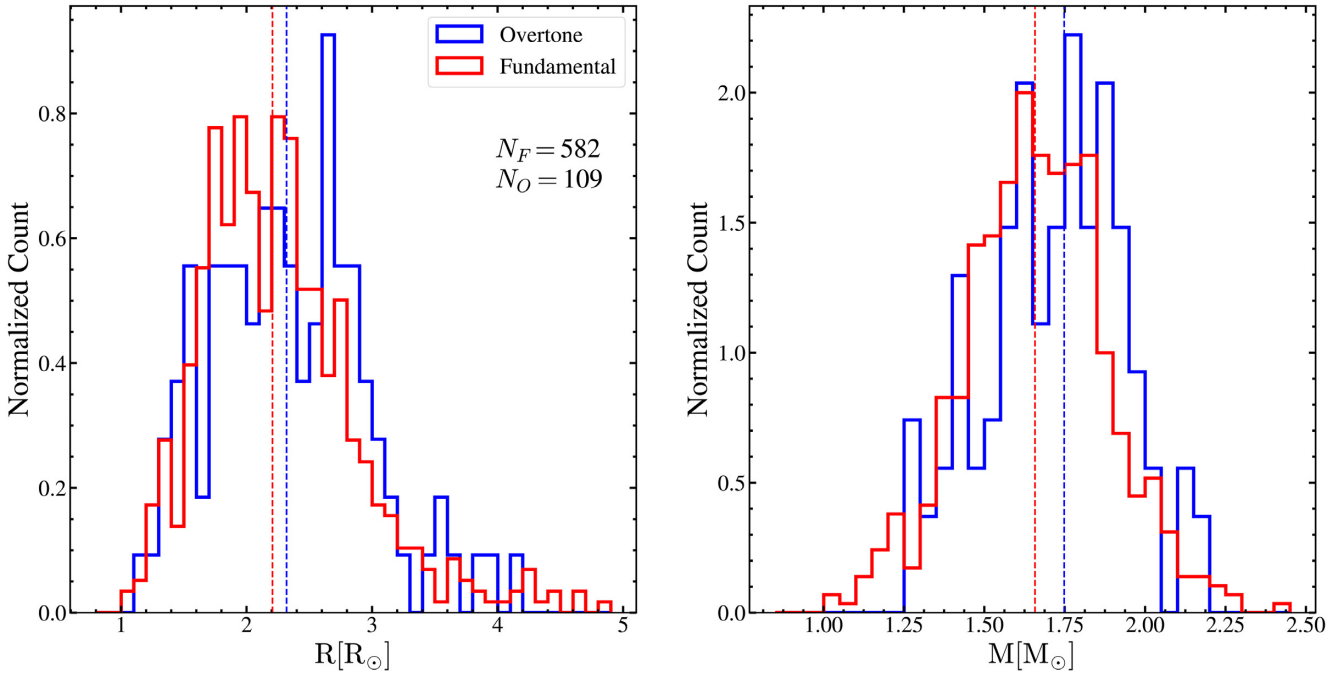

Figure 13. Distributions of radii (left) and masses (right) of the fundamental mode (red) and overtone (blue) δ Scuti stars. The median value for each parameter is illustrated with a dashed line.

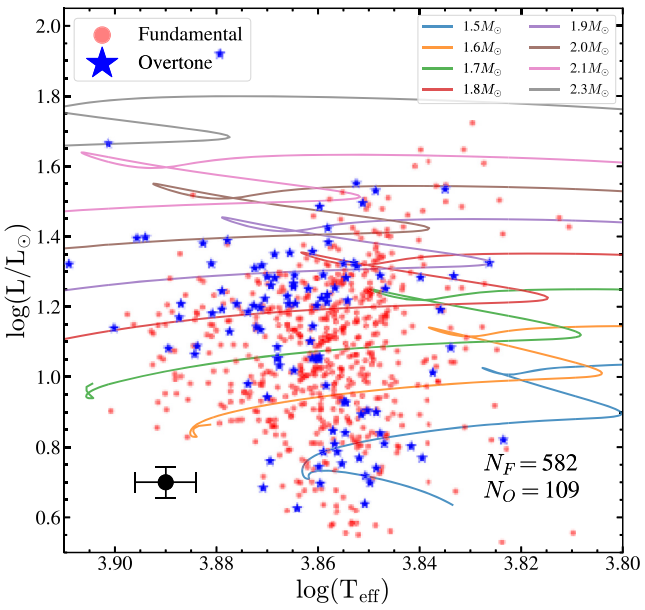

Figure 14. Hertzsprung–Russell diagram for the spectroscopic sub-sample of the fundamental mode and overtone pulsators. Solar metallicity stellar evolution tracks from MIST (Choi et al. 2016; Dotter 2016) are shown for comparison.

`lax/parallax_error` >5. The distributions of the fundamental ($N = 582$) and overtone ($N = 109$) δ Scuti stars in log(g) and [Fe/H] are consistent with each other. The median $T_{\rm eff}$ for the overtone sources is lower than the median $T_{\rm eff}$ for the fundamental mode sources by ∼60 K, but this difference is small given the typical uncertainties in the $T_{\rm eff}$ measurements. SX Phoenicis (SX Phe) stars are considered the type II analogues of the δ Scuti stars with typical metallicities [Fe/H] < -1 (McNamara 1995; Cohen & Sarajedini 2012). From the cross-matches, 15 had [Fe/H] < -1; thus, we estimate the contamination rate of the SX Phe variables as ∼1.5 per cent. On average, the δ Scuti stars with spectroscopic data have median [Fe/H]~ -0.11, log(g)∼4.0, and $T_{\rm eff}$∼7250 K.

We further look at the correlations between these spectroscopic parameters in Fig. 12. We compare the observed data with the MIST stellar evolution models described in Section 3.1. These models agree very well with the observed values of $T_{\rm eff}$ and log(g). Most of our sources have $T_{\rm eff}$ and log(g) consistent with stars having masses $M < 2.1$ M$_\odot$. We use the calibrations from Torres, Andersen & Giménez (2010) to derive the masses and radii of the δ Scuti stars in the spectroscopic sub-sample using $T_{\rm eff}$, log(g), and [Fe/H]. The luminosities are then derived using the radius and $T_{\rm eff}$. Fig. 13 shows the distribution of masses and radii of these sources. The median radii of the fundamental mode and overtone pulsators are similar, with $\langle R_{\rm fundamental}\rangle \sim 2.2$ R$_\odot$ and $\langle R_{\rm overtone}\rangle \sim 2.3$ R$_\odot$. The distribution of masses of the overtone sources seems to suggest an excess of sources at higher mass bins ($M > 1.75$ M$_\odot$) than the fundamental mode pulsators, which is consistent with the position of these stars in the *Gaia* DR2 CMD. The median masses of the fundamental mode and overtone pulsators are slightly different, with $\langle M_{\rm fundamental}\rangle \sim 1.66$ M$_\odot$ and $\langle M_{\rm overtone}\rangle \sim 1.75$ M$_\odot$. However, we note that this difference is small given the uncertainties of the masses derived using the Torres et al. (2010) calibration. Fig. 14 shows the Hertzsprung–Russell diagram for these sources. These data are also consistent with most of these sources having masses $M < 2.1$ M$_\odot$.

In Fig. 12, there is a strong correlation between period and composition. Fundamental mode δ Scuti stars with near-Solar metallicities have longer periods than lower metallicity sources. Fig. 15 shows the dependence of the median metallicity on $\log_{10}(P/{\rm days})$ for both the fundamental mode and overtone pulsators. Linear fits give

$$[{\rm Fe/H}]_{\rm F} = 0.905(\pm 0.062)\log_{10}(P/0.1\,{\rm d}) - 0.116(\pm 0.011), \quad (4)$$

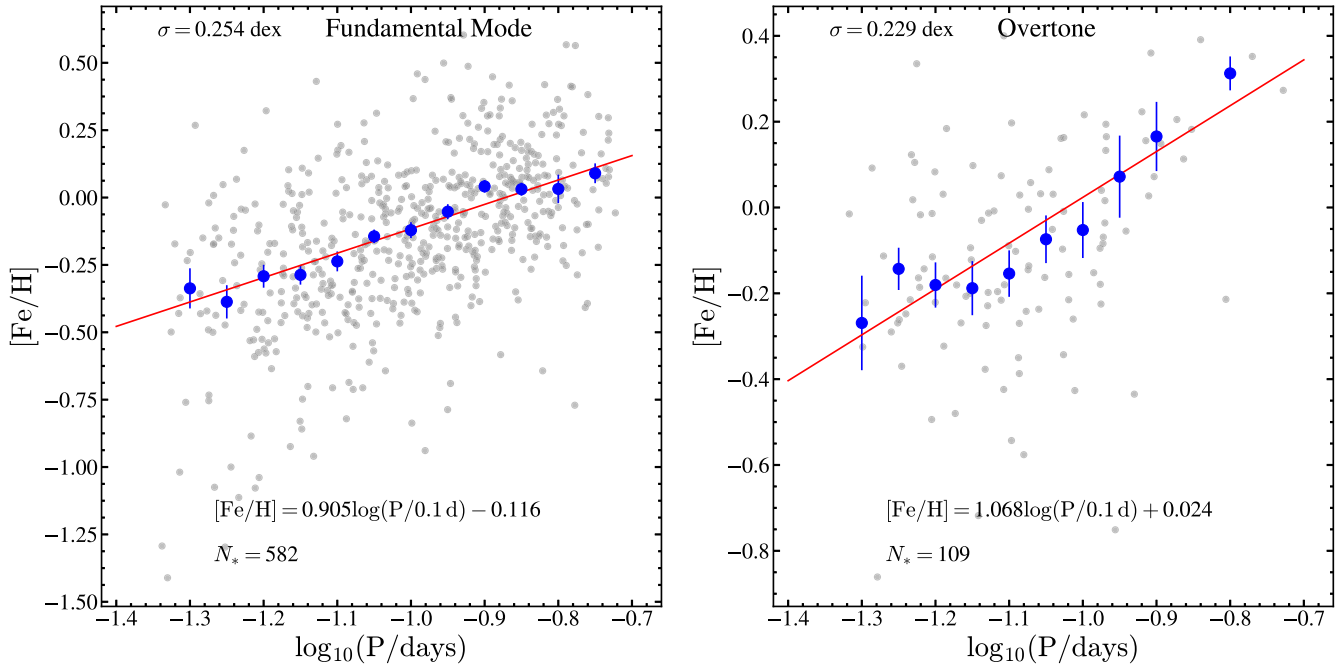

Figure 15. Distribution of median metallicity with $\log_{10}(P/\mathrm{days})$ for the fundamental mode (left) and overtone (right) pulsators. The individual fundamental mode and overtone pulsators used in the binning are shown in grey. A linear fit to the binned data is shown in red.

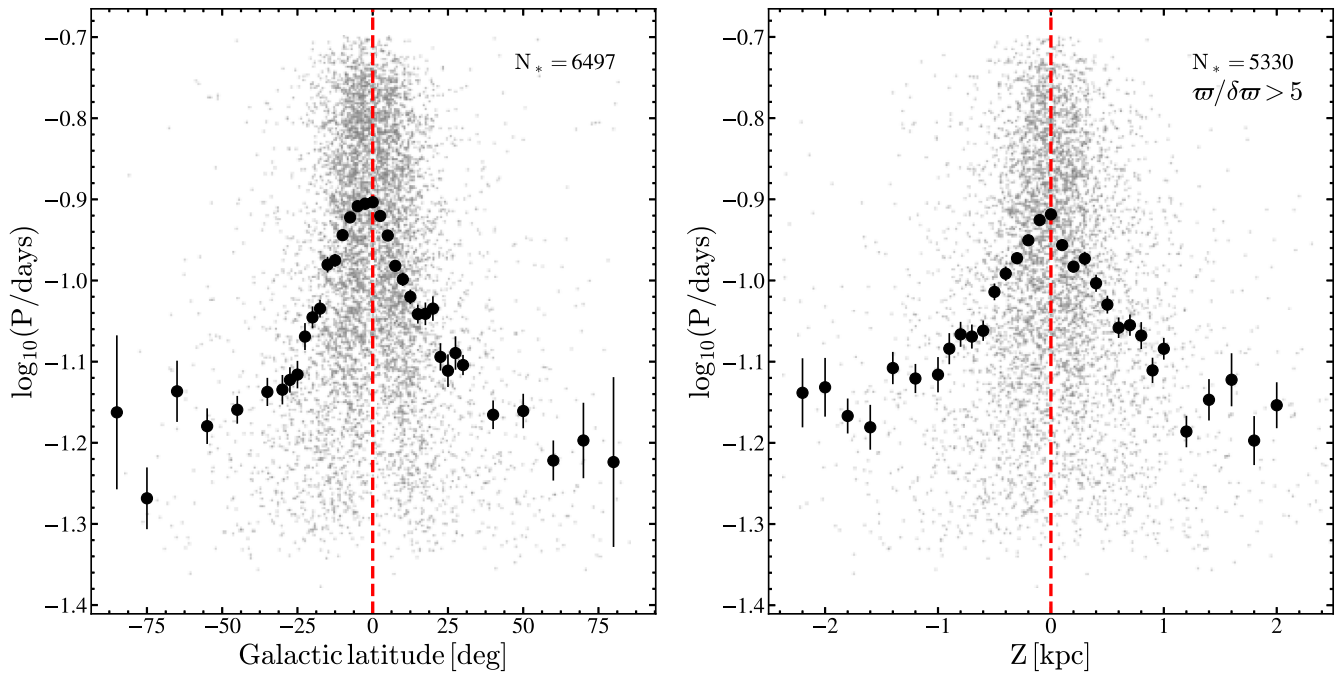

Figure 16. Distribution of median periods with Galactic latitude (left) in bins of 2.5 deg ($-30\,\mathrm{deg} \leq b \leq 30\,\mathrm{deg}$) and 10 deg ($|b| > 30\,\mathrm{deg}$), and the distance from the Galactic mid-plane (right) in bins of 100 pc ($-1\,\mathrm{kpc} \leq Z \leq 1\,\mathrm{kpc}$) and 200 pc ($|Z| > 1\,\mathrm{kpc}$). The individual δ Scuti stars used in the binning are shown in grey.

for the fundamental mode and

$$[\mathrm{Fe/H}]_{\mathrm{O}} = 1.068(\pm0.134)\log_{10}(P/0.1\,\mathrm{d}) + 0.024(\pm0.022), \quad (5)$$

for the overtone pulsators. These relationships both have large scatter ($\sigma \sim 0.25$ dex). The [Fe/H]–$\log_{10}(P/\mathrm{days})$ slopes of the two fits are consistent given the uncertainties, but the zero-points differ as expected. At any given period, the overtone pulsators have a higher metallicity than fundamental mode pulsators of the same period.

The median period varies significantly with metallicity, from $\log_{10}(P/\mathrm{days}) \sim -1.1$ for sources with [Fe/H] < -0.3 to $\log_{10}(P/\mathrm{days}) \sim -0.9$ for sources with supersolar metallicities [Fe/H] > 0. This is reflected in the positions of the δ Scuti stars in the Galaxy (Fig. 2). Sources closer to the Galactic disc, which should have higher metallicities (Pedicelli et al. 2009), tend to have longer

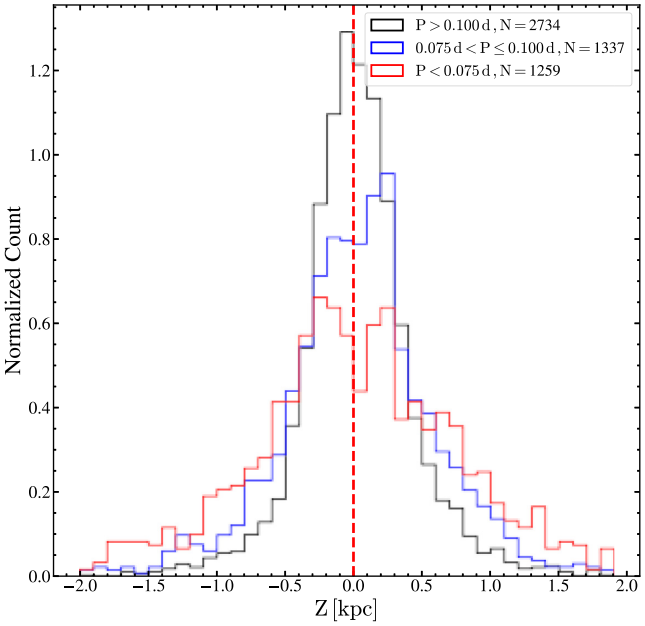

Figure 17. Distribution of the distances from the Galactic mid-plane in bins of 100 pc (-1 kpc $\leq Z \leq 1$ kpc) and 200 pc ($|Z| > 1$ kpc) for δ Scuti stars with periods $P < 0.075$ d (red), 0.075 d $< P \leq 0.100$ d (blue), and $P > 0.100$ d (black).

periods than sources further away from the disc (Fig. 16). Thus, the δ Scuti period gradient in Galactic latitude is likely due to the vertical metallicity gradient of the Galactic disc. To characterize this effect further, we calculate the cylindrical Galactocentric coordinates (R and Z) for these sources using the *Gaia* DR2 distances (parallaxes better than 20 per cent) and the `astropy` coordinate transformations. Fig. 16 shows the median periods as a function of the distance from the Galactic mid-plane (Z) in bins of 100 pc (-1 kpc $\leq Z \leq 1$ kpc) and 200 pc ($|Z| > 1$ kpc). It is evident that towards the Galactic disc, the median period increases, whereas towards the halo, the median period drops sharply. Fig. 17 shows the distribution of distances from the Galactic mid-plane for δ Scuti stars with periods $P < 0.075$ d, 0.075 d $< P \leq 0.100$ d, and $P > 0.100$ d. We find that there is an excess of sources with short periods ($P < 0.100$ d) away from the Galactic disc ($|Z| > 0.5$ kpc) when compared to the sources with longer periods. This effect is more pronounced at even shorter periods as the sources with $P < 0.075$ d have a broader distribution in Z than the sources with 0.075 d $< P \leq 0.100$ d. Stars with $P > 0.100$ d are predominantly located close to the Galactic disc ($|Z| < 0.5$ kpc).

This could potentially be an observational bias related to the decreasing sensitivity to lower luminosity (i.e. shorter period) δ Scuti stars towards the Galactic disc due to extinction. To investigate this further, we examined the distributions of W_{JK} magnitudes along with the distributions of the median period with distance from the Galactic mid-plane in extinction bins of $A_V < 0.5$ mag, 0.5 mag $< A_V \leq 1$ mag, and $A_V > 1$ mag. Here, we used variable binning in Z as the sources with high extinctions ($A_V > 0.5$ mag) are largely located towards the disc ($|Z| < 1$ kpc), whereas the sources with small extinctions are located away from the disc. The same trend observed in Fig. 16 is reproduced in all the extinction bins.

As a check on the vertical metallicity gradient explaining the vertical trend in period, we can examine the trend for RR Lyrae stars. Metal-rich RRab stars have shorter periods (Sandage 1993; Beaton et al. 2018), so a vertical metallicity gradient should lead to a reversed trend in period with Z from the δ Scuti. We selected a sample of fundamental mode RR Lyrae (RRAB) stars from the ASAS-SN catalogue with `parallax/parallax_error` >3, and we see exactly this reversed correlation in Fig. 18. We will explore such trends further in Jayasinghe et al. (2020, in prep.).

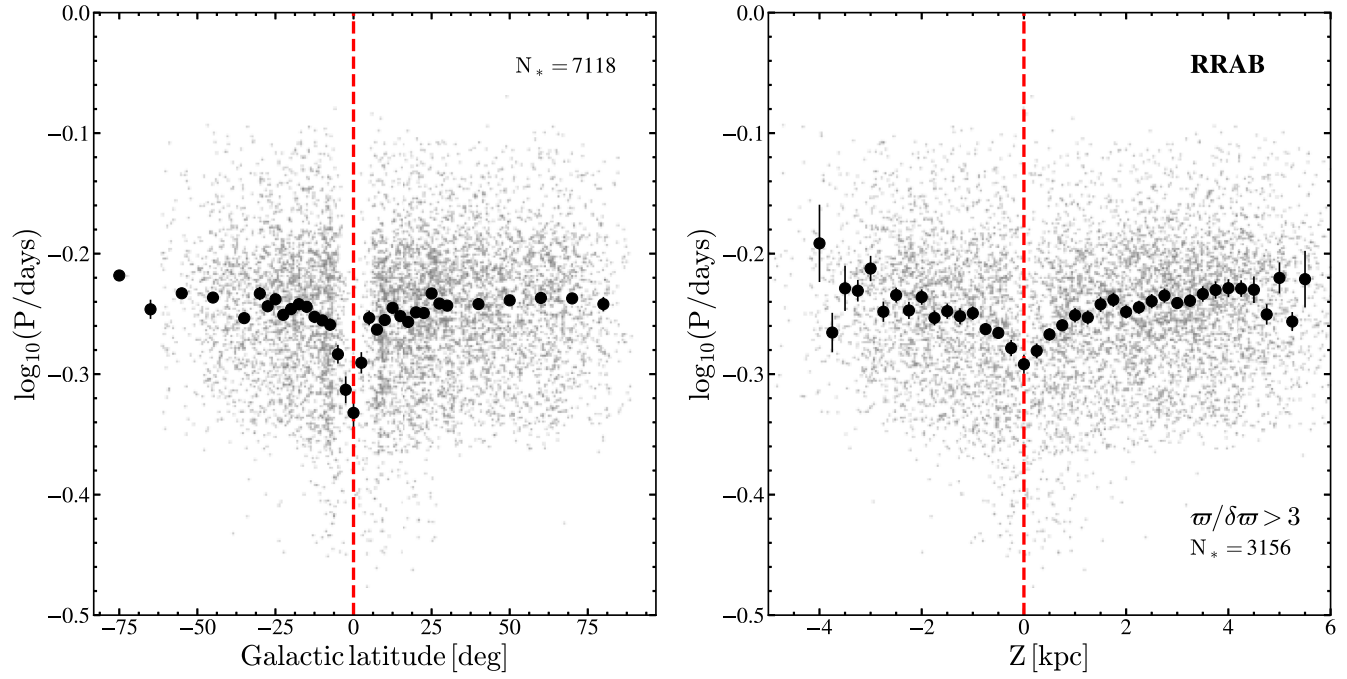

Figure 18. Distribution of the median periods of fundamental mode RR Lyrae stars (RRab) with Galactic latitude (left) in bins of 2.5 deg (-30 deg $\leq b \leq 30$ deg) and 10 deg ($|b| > 30$ deg), and the distance from the Galactic mid-plane (right) in bins of 250 pc (-3.5 kpc $\leq Z \leq 4$ kpc). The individual RRab stars used in the binning are shown in grey. As expected, this is the opposite trend seen in δ Scuti stars (Fig. 16).

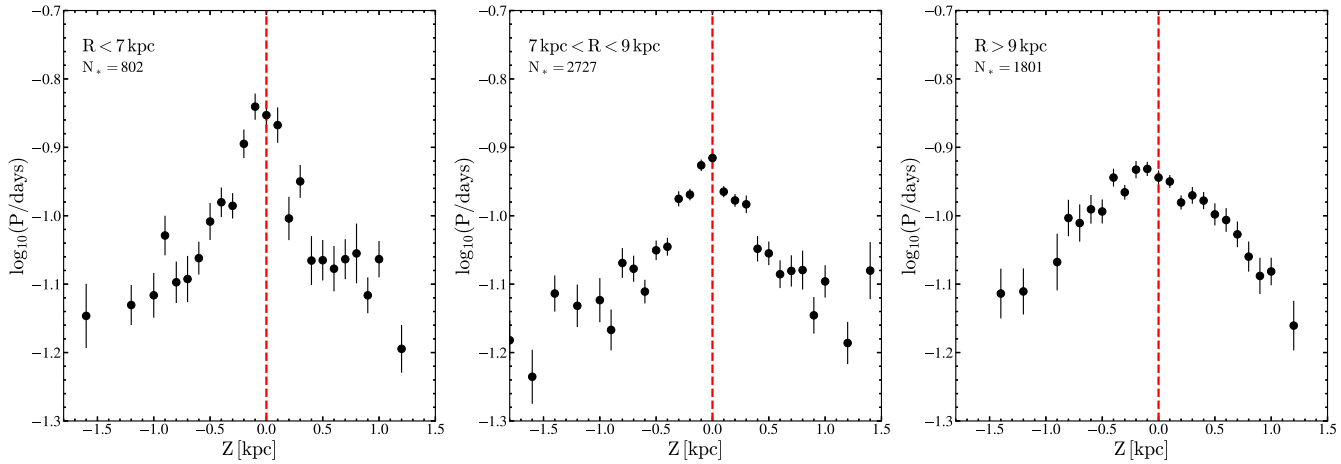

Figure 19. Distribution of median periods with distances from the Galactic mid-plane in three bins of Galactocentric radius with $R < 7$ kpc (left), $7\,\mathrm{kpc} < R < 9\,\mathrm{kpc}$ (centre), and $R > 9$ kpc (right).

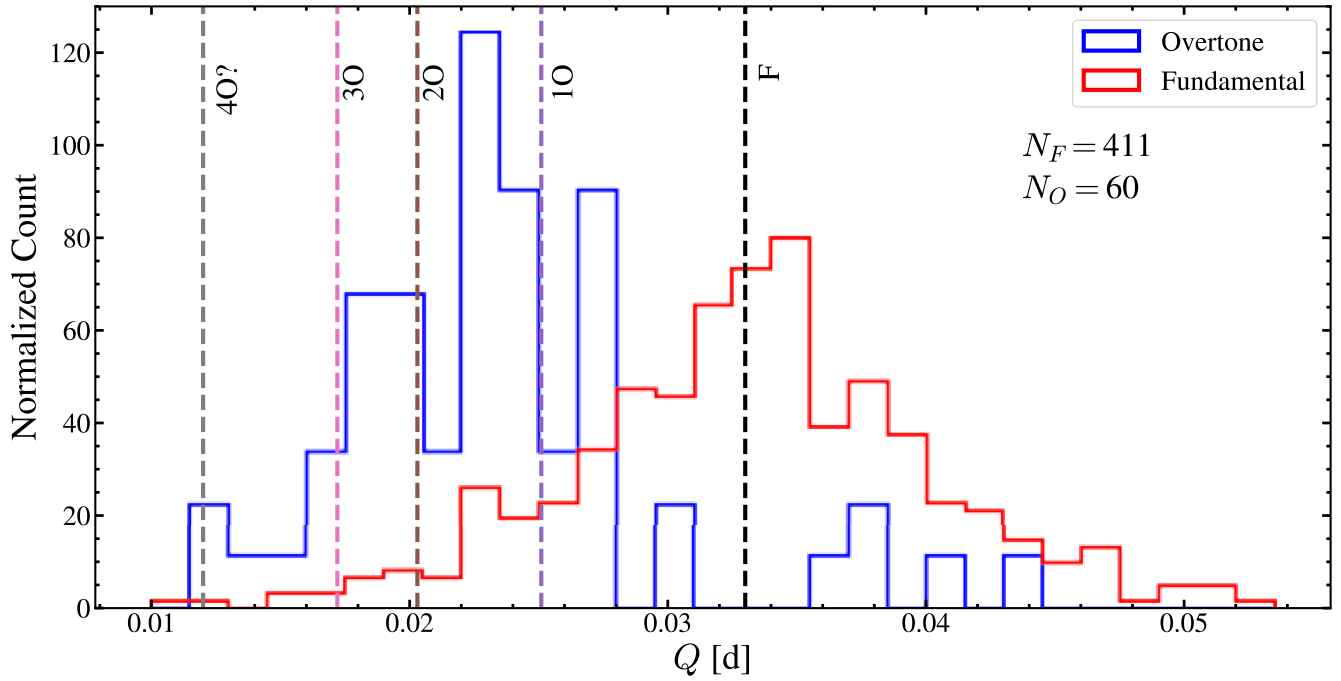

Figure 20. Distribution of the pulsational constants (Q) for the sources in the spectroscopic sub-sample. The expected Q values for the fundamental mode and different overtone modes from North et al. (1997) are also shown for reference.

Fig. 19 shows the median periods as a function of the distance from the Galactic mid-plane (Z) in bins of 100 pc ($-1\,\mathrm{kpc} \leq Z \leq 1\,\mathrm{kpc}$) and 200 pc ($|Z| > 1\,\mathrm{kpc}$) for sources with Galactocentric radii $R < 7\,\mathrm{kpc}$, $7\,\mathrm{kpc} < R < 9\,\mathrm{kpc}$, and $R > 9\,\mathrm{kpc}$. We see that at fixed $|Z|$, stars at lower Galactocentric radii have longer periods, consistent with the expected radial gradient of metallicity (Pedicelli et al. 2009). The trends are harder to illustrate, however, because the stars span a limited fractional range in R and there are strong correlations between R and the average height above the plane. The median period at $Z{\sim}0$ increases from $\log_{10}(P/\mathrm{days}){\sim} -0.94$ in the bin $R > 9\,\mathrm{kpc}$ to $\log_{10}(P/\mathrm{days}){\sim} -0.85$ in the bin $R < 7\,\mathrm{kpc}$. We also find that the widths of these distributions broaden with increasing distance from the Galactic centre, which is consistent with our finding that longer period δ Scuti stars are more likely to be located towards regions with higher metallicity.

With measurements of $T_{\rm eff}$ and $\log(g)$, we are also able to calculate the pulsational constant

$$Q = P\sqrt{\frac{\bar{\rho}}{\bar{\rho}_{\odot}}},$$

where P is the period in days and $\bar{\rho}/\bar{\rho}_{\odot}$ is the mean stellar density normalized by the mean Solar density (Bowman 2017). This can be rewritten as

$$\log(Q) = \log(P) + 0.5\log(g) + 0.1M_{\rm bol} + \log(T_{\rm eff}) - 6.454,$$

where $M_{\rm bol} = M_V - A_V + BC$ is the absolute bolometric magnitude of the source (Bowman 2017). We derived the bolometric correction for these sources using the `isochrones` package (Morton 2015),

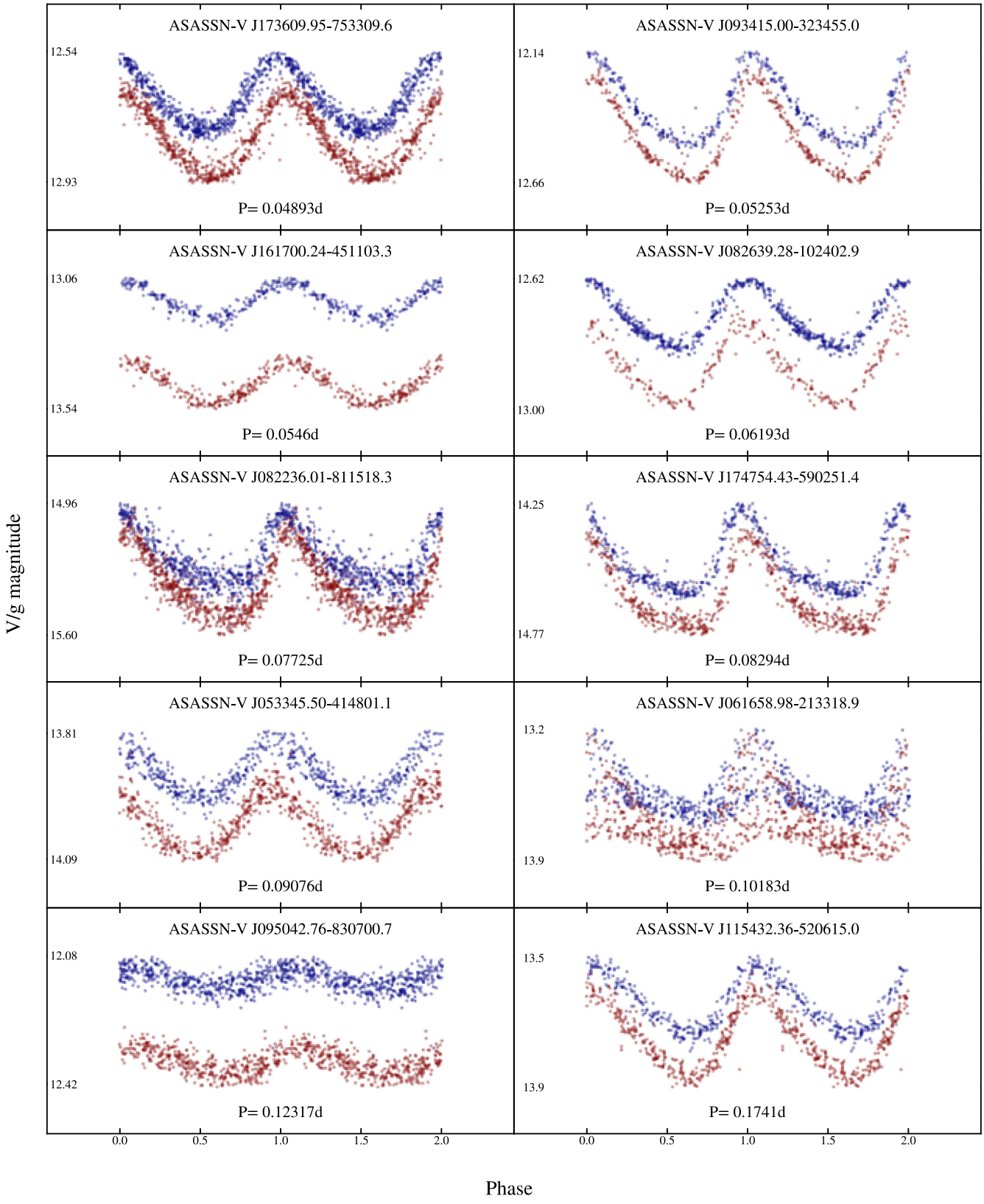

Figure 21. Phased ASAS-SN light curves for the 10 fundamental mode δ Scuti stars in the Southern hemisphere with the *TESS* data. The light curves are scaled by their minimum and maximum *V*/*g*-band magnitudes. The blue points correspond to *g*-band data and the red points correspond to *V*-band data.

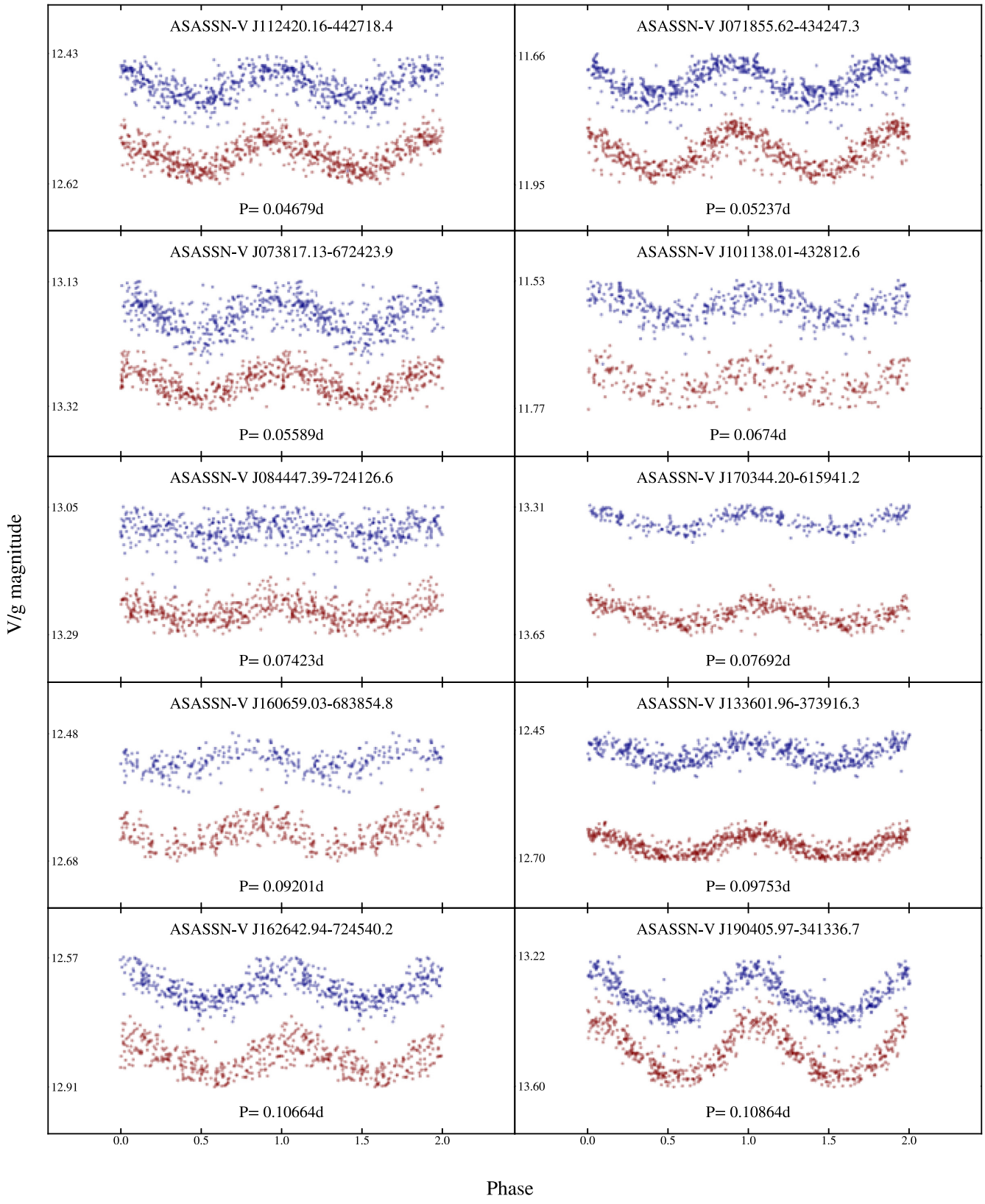

Figure 22. Phased ASAS-SN light curves for the 10 overtone δ Scuti stars in the Southern hemisphere with the *TESS* data. The format is the same as Fig. 21.

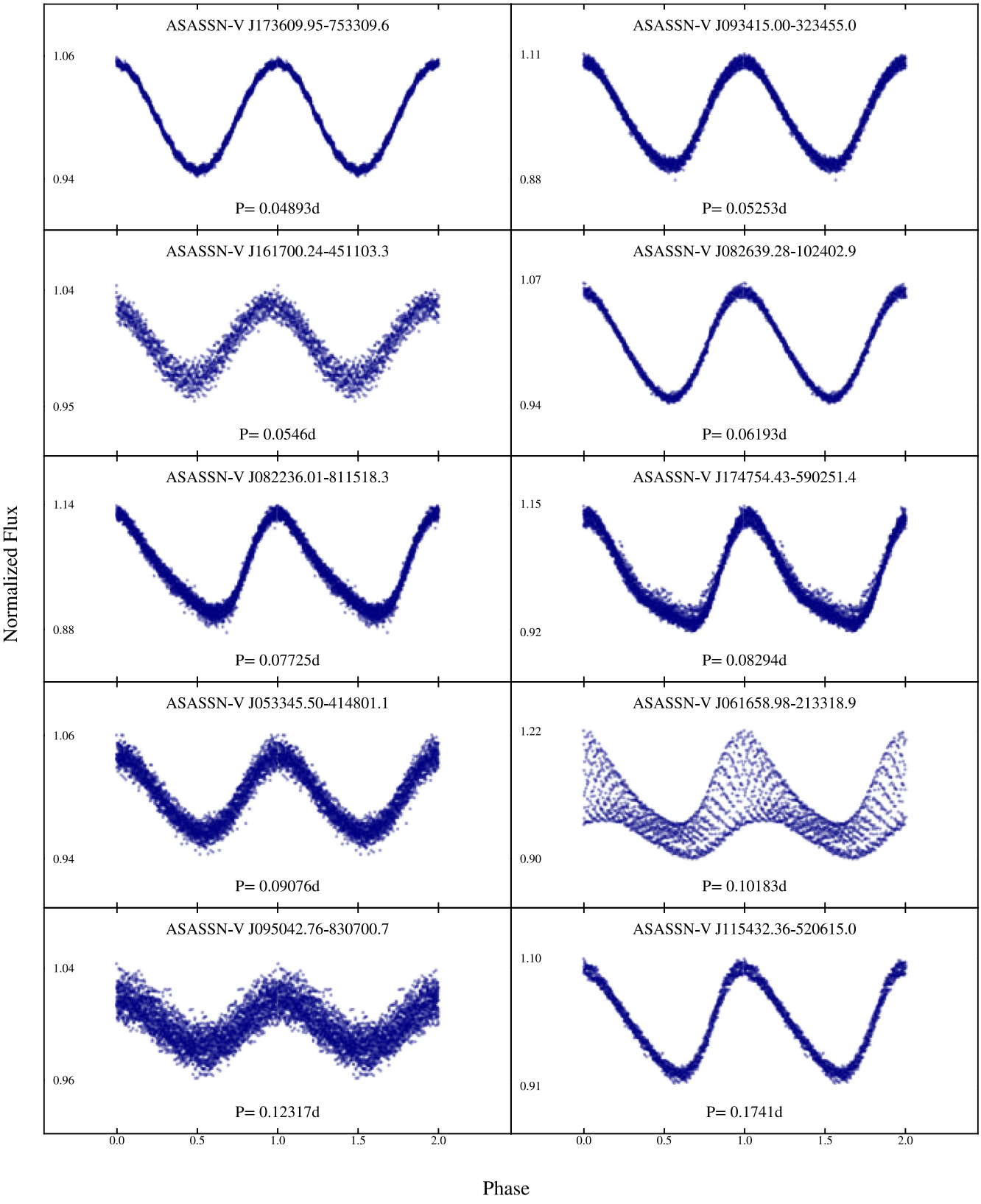

Figure 23. Phased *TESS* light curves for the 10 fundamental mode δ Scuti stars in the Southern hemisphere with the *TESS* data. The light curves are scaled by their minimum and maximum variations in flux.

Table 3. Summary of the 10 fundamental mode and 10 overtone δ Scuti stars in the Southern hemisphere with the *TESS* data.

ASAS-SN ID	RAJ2000	DEJ2000	Period (d)	$A_{\rm RFR}$ (mag)	Type	ΔW_{JK} (mag)	V (mag)	T (mag)
J162642.94−724540.2	246.6789	−72.761 17	0.106 638	0.13	Overtone	−0.68	12.59	12.20
J084447.39−724126.6	131.197 46	−72.690 72	0.074 229	0.07	Overtone	−1.34	13.06	12.67
J160659.03−683854.8	241.745 97	−68.648 55	0.092 009	0.06	Overtone	−0.72	12.49	12.16
J073817.13−672423.9	114.571 36	−67.406 63	0.055 886	0.08	Overtone	−0.96	13.18	12.82
J170344.20−615941.2	255.934 15	−61.994 79	0.076 917	0.07	Overtone	−0.95	13.33	12.90
J112420.16−442718.4	171.084 01	−44.455 10	0.046 792	0.07	Overtone	−1.17	12.46	12.23
J071855.62−434247.3	109.731 77	−43.713 13	0.052 369	0.09	Overtone	−1.39	11.71	11.29
J101138.01−432812.6	152.908 38	−43.470 16	0.067 405	0.07	Overtone	−1.12	11.58	11.19
J133601.96−373916.3	204.008 15	−37.654 52	0.097 528	0.06	Overtone	−0.80	12.49	12.11
J190405.97−341336.7	286.024 88	−34.226 87	0.108 644	0.16	Overtone	−0.73	13.34	12.97
J095042.76−830700.7	147.678 15	−83.116 86	0.123 165	0.08	Fundamental	0.16	12.17	11.69
J082236.01−811518.3	125.650 04	−81.255 08	0.077 246	0.40	Fundamental	−0.24	15.19	14.77
J173609.95−753309.6	264.041 46	−75.552 66	0.048 927	0.23	Fundamental	−0.04	12.59	12.32
J174754.43−590251.4	266.976 81	−59.047 60	0.082 942	0.34	Fundamental	−0.39	14.39	13.95
J115432.36−520615.0	178.634 82	−52.104 17	0.174 102	0.23	Fundamental	0.20	13.61	13.19
J161700.24−451103.3	244.251 01	−45.184 24	0.054 598	0.16	Fundamental	−0.07	13.15	12.22
J053345.50−414801.1	83.439 60	−41.800 30	0.090 756	0.15	Fundamental	−0.04	13.90	13.56
J093415.00−323455.0	143.562 49	−32.581 94	0.052 528	0.36	Fundamental	0.07	12.37	12.14
J061658.98−213318.9	94.245 76	−21.555 26	0.101 825	0.40	Fundamental	−0.04	13.55	13.28
J082639.28−102402.9	126.663 67	−10.400 81	0.061 929	0.20	Fundamental	−0.24	12.72	12.42

which utilizes the MIST bolometric correction grids (Choi et al. 2016; Dotter 2016).

Fig. 20 shows the distribution of Q for both the fundamental mode and overtone pulsators in the spectroscopic sub-sample. The expected values of Q for the fundamental and overtone modes estimated by North, Jaschek & Egret (1997) are also shown for reference. The calculation of Q is strongly dependent on the stellar parameters (Breger et al. 1990; Bowman 2017), and the fractional uncertainties in Q can be rather large ($\gtrsim$15 per cent). Nevertheless, there is a clear distinction between the overtone pulsators and the fundamental mode pulsators. Most of the fundamental mode pulsators have Q values close to the expected value for the radial fundamental mode ($Q_F \sim 0.033$ d), but there is also evidence that some of these sources pulsate in the first overtone ($Q_{1O} \sim 0.0255$ d). This suggests that some fraction of the sources classified as fundamental mode pulsators actually have a dominant period corresponding to the first overtone. This was already hinted at in Fig. 7. This uncertainty in the dominant pulsational mode between fundamental mode and first overtone pulsators adds to the scatter in the derived PLRs for the fundamental mode pulsators. This problem is difficult to solve with just the ASAS-SN data, as mode identification for a large ensemble of δ Scuti stars, most of which do not have spectroscopic determinations of $T_{\rm eff}$ and log(g) or high-cadence (*Kepler/K2* or *TESS*) data, is challenging. Overtone pulsators in the spectroscopic sub-sample form a distinct population in Q, with multiple peaks corresponding to the first overtone, second overtone ($Q_{2O} \sim 0.0205$ d), and third overtone ($Q_{3O} \sim 0.0174$ d) visible in the data, and an absence of sources with Q close to the fundamental mode. This is also consistent with our observations in Fig. 7. The sample appears to be dominated by sources pulsating in the first overtone, followed by sources pulsating in the second and third overtones. We also note a peak centred at ($Q \sim 0.012$ d) that could be the fourth overtone, but we were unable to find a prediction for this mode's Q in the literature.

5 δ SCUTI STARS IN *TESS*

The *TESS* (Ricker et al. 2015) is currently observing most of the sky with a baseline of at least 27 d and has finished observations in the Southern hemisphere. Antoci et al. (2019) presented the first asteroseismic results for δ Scuti and γ Dor stars observed in the *TESS* mission, utilizing the 2 min cadence light curves in Sectors 1 and 2. As an experiment, we extracted *TESS* light curves of 10 fundamental and 10 overtone stars in the Southern hemisphere.

We analyse the *TESS* data using an image subtraction pipeline optimized for use with the full frame images (FFIs). This pipeline is derived from that used to process the ASAS-SN data, and is based on the ISIS package (Alard & Lupton 1998; Alard 2000). This technique has previously been applied successfully to *TESS* observations of a wide range of astrophysical objects including supernovae (Fausnaugh et al. 2019; Vallely et al. 2019), tidal disruption events (Holoien et al. 2019), young stellar objects (Hodapp et al. 2019), and the most extreme heartbeat star yet discovered (Jayasinghe et al. 2019c). For each sector, we constructed a reference image from the first 100 FFIs of good quality obtained during that sector, excluding those with sky background levels or PSF widths above average for the sector. FFIs associated with non-zero data quality flags were also excluded. The primary outcome of this procedure is the exclusion of FFIs obtained during spacecraft momentum dumps (quality flag value 32) and those obtained during epochs heavily impacted by stray Earthlight or Moonlight (quality flag value 2048).

While the image subtraction technique is well suited to producing differential light curves, the large pixel scale of *TESS* makes it difficult to obtain reliable measurements of the flux of a given source in the reference image. Instead of relying on this, we have estimated the reference flux using the `ticgen` software package (Jaffe & Barclay 2017; Stassun et al. 2018). The *TESS*-band magnitude estimates from `ticgen` were converted into fluxes using an instrumental zero-point of 20.44 electrons per second in the FFIs, based on the values provided in the *TESS* Instrument Handbook (Vanderspek et al. 2018). Flux was then added to the raw differential light curves such that the median of each target's observations matched the estimated reference value. This allowed us to produce the normalized flux light curves shown in Figs 23 and 24. The light curves do not include epochs where the observations were compromised by scattered light artefacts from the Earth or Moon.

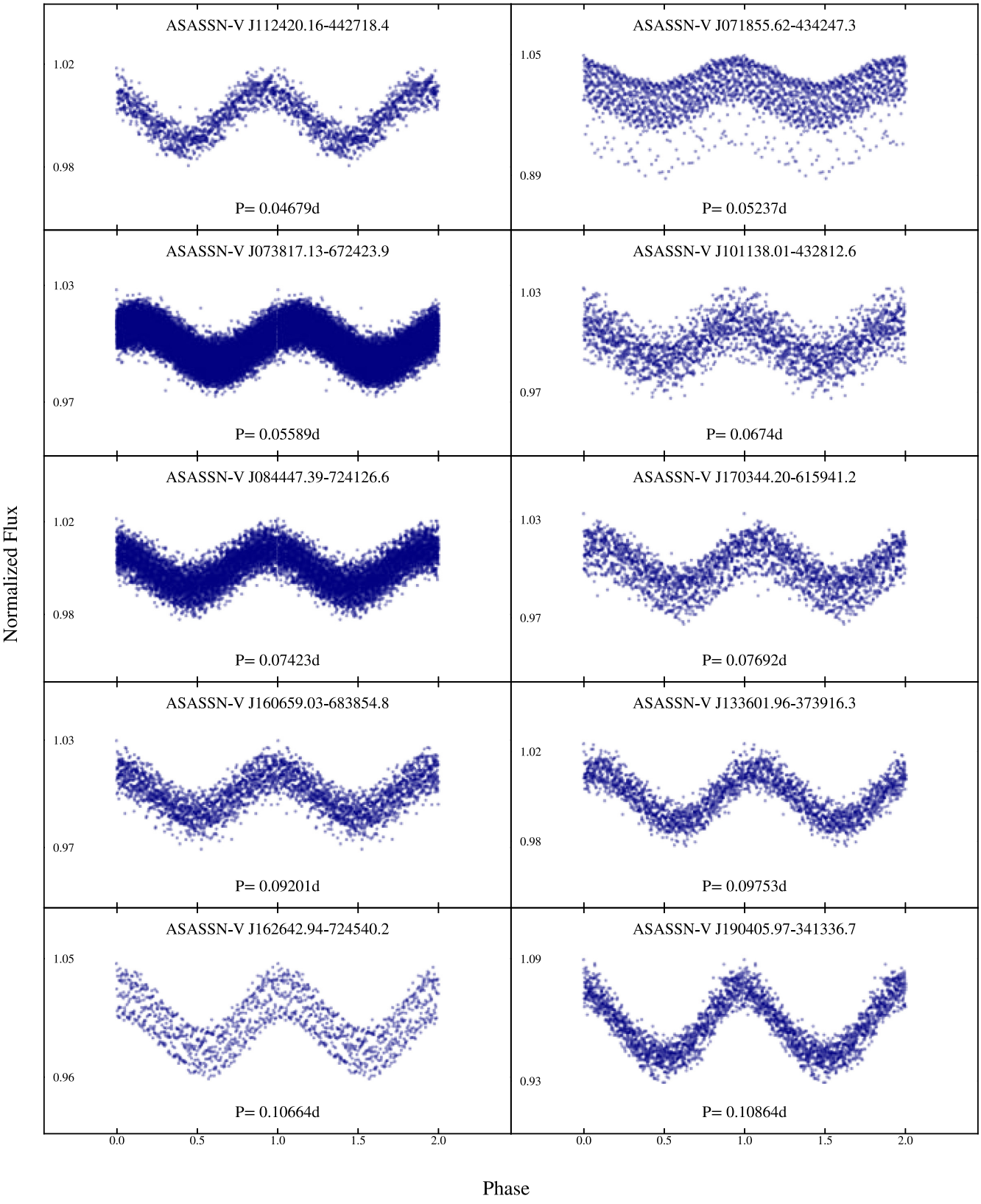

Figure 24. Phased *TESS* light curves for the 10 overtone δ Scuti stars in the Southern hemisphere with the *TESS* data. The format is the same as Fig. 23.

Table 4. Pulsation frequencies, amplitudes, and SNRs of the 10 fundamental mode δ Scuti stars in the Southern hemisphere with the *TESS* data.

ASAS-SN ID	Frequency (d^{-1})	Amplitude (ppt)	SNR	Comment
J093415.00−323455.0				
	19.037 813 ± 0.000 011	95.07 ± 0.23	19.4	–
	9.925 218 ± 0.000 158	6.33 ± 0.09	5.7	–
J082639.28−102402.9				
	16.147 136 ± 0.000 047	54.76 ± 0.48	15.6	–
	20.042 744 ± 0.001 156	2.25 ± 0.16	5.6	–
J174754.43−590251.4				
	12.056 074 ± 0.000 018	86.75 ± 0.67	26.1	–
	23.887 109 ± 0.000 066	24.21 ± 0.17	16.3	–
J061658.98−213318.9				
	9.820 608 ± 0.000 042	68.54 ± 0.15	14.5	f_0
	12.698 695 ± 0.000 044	63.64 ± 1.25	14.3	f_1
	2.878 137 ± 0.000 108	26.27 ± 0.13	13.7	$f_1 - f_0$
	19.641 166 ± 0.000 253	11.26 ± 0.13	10.7	$2f_0$
	22.517 004 ± 0.000 114	19.14 ± 1.10	10.6	$f_1 + f_0$
	6.942 471 ± 0.000 418	6.81 ± 0.13	7.7	$2f_0 - f_1$
	15.579 131 ± 0.000 504	5.65 ± 0.13	6.6	$2f_1 - f_0$
	22.602 061 ± 0.000 289	10.84 ± 0.15	6.0	–
	15.659 590 ± 0.000 829	3.42 ± 0.13	4.0[a]	–
	18.533 129 ± 0.001 851	1.53 ± 0.14	2.5[a]	$3f_1 - 2f_0$
J082236.01−811518.3				
	12.945 750 ± 0.000 015	96.97 ± 1.12	25.5	–
	22.108 528 ± 0.000 063	22.94 ± 0.23	22.4	–
	9.163 372 ± 0.000 532	2.73 ± 0.26	6.1	–
J095042.76−830700.7				
	8.119 214 ± 0.000 038	17.35 ± 0.12	18.5	–
	15.983 336 ± 0.000 203	3.24 ± 0.11	14.2	–
	13.386 403 ± 0.000 323	2.04 ± 0.10	13.8	–
	8.430 682 ± 0.000 079	8.37 ± 0.13	9.0	–
	15.608 756 ± 0.000 323	2.03 ± 0.11	8.4	–
	8.056 102 ± 0.000 130	5.07 ± 0.12	5.4	–
J115432.36−520615.0				
	5.743 287 ± 0.000 040	75.77 ± 0.81	16.1	–
	11.488 557 ± 0.000 224	13.35 ± 0.15	11.0	–
	7.622 044 ± 0.000 428	7.00 ± 0.16	6.6	–
J053345.50−414801.1				
	11.018 842 ± 0.000 036	36.82 ± 0.14	21.5	f_0
	22.037 130 ± 0.000 456	2.91 ± 0.12	12.0	$2f_0$
	18.254 843 ± 0.000 553	2.40 ± 0.14	11.0	–
J173609.95−753309.6				
	20.438 721 ± 0.000 011	51.32 ± 0.07	20.3	–
	7.122 998 ± 0.000 480	1.21 ± 0.05	7.9	NR?[b]
J161700.24−451103.3				
	18.316 320 ± 0.000 076	28.59 ± 0.22	14.9	–
	23.897 836 ± 0.000 806	2.68 ± 0.10	8.3	–

Notes. [a] Detections with SNR<5.
[b] Possible non-radial mode.

These samples of 10 fundamental mode and 10 overtone δ Scuti stars with *TESS* light curves are summarized in Table 3. The phased ASAS-SN *V*- and *g*-band light curves are shown in Fig. 21 (fundamental mode pulsators) and Fig. 22 (overtone pulsators). The phased *TESS* light curves for the same periods are shown in Fig. 23 (fundamental mode pulsators) and Fig. 24 (overtone pulsators).

The light curves of the fundamental mode pulsators are morphologically different from the light curves of the overtone pulsators. The overtone pulsators have more symmetric light curves but generally have multiple excited modes leading to more overall scatter. At this stage, we identified two sources with interesting light curves. ASASSN-V J061658.98−213318.9 has a light curve that suggests the existence of beat frequencies, and ASASSN-V J071855.62−434247.3 has evidence of eclipses.

We used the `Period04` software package (Lenz & Breger 2005) to calculate the discrete Fourier transform of the *TESS* light curves. Each light curve was iteratively whitened until all the frequencies with signal-to-noise ratios (SNRs) >5 were retrieved. We have summarized the results of the frequency analysis in Table 4 (fundamental mode pulsators) and Table 5 (overtone pulsators). As was noted earlier, the pulsational amplitudes of the fundamental mode pulsators are larger than those of the overtone pulsators. In all but two cases, the fundamental mode is the dominant pulsation mode of the fundamental mode sources, and vice versa. However, the vast majority of these sources really are multimode pulsators.

Table 5. Pulsation frequencies, amplitudes, and SNRs of the 10 overtone δ Scuti stars in the Southern hemisphere with the *TESS* data.

ASAS-SN ID	Frequency (d^{-1})	Amplitude (ppt)	SNR	Comment
J073817.13−672423.9				
	17.893 421 ± 0.000 006	9.75 ± 0.05	55.0	–
	18.501 227 ± 0.000 011	5.49 ± 0.04	31.7	–
J160659.03−683854.8				
	10.868 886 ± 0.000 113	11.61 ± 0.08	13.0	–
	9.508 483 ± 0.000 257	5.09 ± 0.09	12.4	–
	11.630 640 ± 0.000 195	6.71 ± 0.08	7.5	–
	6.744 660 ± 0.001 870	0.70 ± 0.07	6.9	–
J133601.96−373916.3				
	10.253 547 ± 0.000 151	11.12 ± 0.09	12.8	–
	7.586 851 ± 0.000 430	3.91 ± 0.16	7.9	–
J162642.94−724540.2				
	9.378 243 ± 0.000 124	21.69 ± 0.11	9.3	–
	12.036 304 ± 0.000 165	16.24 ± 0.10	9.2	–
	17.812 164 ± 0.001 497	1.79 ± 0.10	5.7	–
	21.122 983 ± 0.001 309	2.05 ± 0.11	5.5	–
J112420.16−442718.4				
	21.369 170 ± 0.000 167	10.23 ± 0.23	13.7	–
	18.381 295 ± 0.000 518	3.29 ± 0.08	8.6	–
	16.744 625 ± 0.000 914	1.87 ± 0.08	8.4	–
J101138.01−432812.6				
	14.835 528 ± 0.000 235	11.03 ± 0.14	14.5	–
	7.242 484 ± 0.000 564	4.61 ± 0.14	9.4	–
	12.390 962 ± 0.000 346	7.50 ± 0.13	8.1	–
	11.837 701 ± 0.000 386	6.72 ± 0.14	7.5	–
	7.088 432 ± 0.000 991	2.62 ± 0.13	5.4	–
J190405.97−341336.7				
	9.204 886 ± 0.000 110	45.52 ± 0.29	15.4	–
	14.201 801 ± 0.000 759	6.58 ± 0.25	10.3	–
	11.958 898 ± 0.000 873	5.72 ± 0.28	9.1	–
	18.407 353 ± 0.001 206	4.14 ± 0.29	7.6	–
	6.190 006 ± 0.001 103	4.53 ± 0.26	5.5	–
J084447.39−724126.6				
	13.471 703 ± 0.000 030	7.95 ± 0.05	23.6	–
	12.146 557 ± 0.000 070	3.35 ± 0.05	16.8	–
	12.964 131 ± 0.000 054	4.35 ± 0.06	12.4	–
	15.226 689 ± 0.000 209	1.13 ± 0.05	10.5	–
J071855.62−434247.3				
	19.095 246 ± 0.000 102	18.16 ± 0.10	15.3	–
	0.765 662 ± 0.000 059	31.55 ± 0.10	11.7	$P_{orb}/2$, P_{orb} = 2.6096 d
J170344.20−615941.2				
	13.001 638 ± 0.000 199	12.82 ± 0.21	15.4	–
	23.413 779 ± 0.001 242	2.06 ± 0.14	7.9	–
	0.394 516 ± 0.000 274	9.32 ± 0.14	6.5	P_{orb}, P_{orb} = 2.5347 d

The remarkable light curve of the source ASASSN-V J061658.98−213318.9 is composed of two dominant pulsation modes $f_0 = 9.820\,608 d^{-1}$ and $f_1 = 12.698\,695 d^{-1}$ with a period ratio $P_1/P_0 = 0.773$ that suggests that f_1 is the first overtone. There is also a remarkable array of high-amplitude beat frequencies detected at $f_1 - f_0, f_1 + f_0, 2f_0, 2f_0 - f_1, 2f_1 - f_0$, and $3f_1 - 2f_0$. The last beat frequency was nominally below our SNR threshold of SNR = 5.

We also identify that two new δ Scuti eclipsing binaries, ASASSN-V J071855.62−434247.3 and ASASSN-V J170344.20−615941.2, were both in the sample of overtone pulsators and have short orbital periods of $P_{orb} = 2.6096$ d and $P_{orb} = 2.5347$ d, respectively. Fig. 25 separately shows the pulsational and eclipsing components of these two systems. We retrieved numerous orbital harmonics with SNR below our threshold (up to $N = 14$) from the light curve of ASASSN-V J071855.62−434247.3, which were used to construct the eclipsing component shown in Fig. 25. The eclipsing component of ASASSN-V J071855.62−434247.3 has a strong ellipsoidal component with sharp eclipses, whereas ASASSN-V J170344.20−615941.2 appears to be a semidetached eclipsing system. Such eclipsing binaries can be powerful tools for probing the internal structure of stars, but only ∼100 such δ Scuti eclipsing binaries are currently known (Kahraman Aliçavus et al. 2017).

Fig. 26 shows a Petersen diagram (Petersen 1973) comparing the longer, fundamental period P_L to the period ratio P_S/P_L with a secondary, shorter period P_S. For the fundamental mode stars, we define P_S to be the highest amplitude higher frequency period. For the overtone stars, we were only able to clearly identify the fundamental mode from the light curves for two sources, ASASSN-V J160659.03−683854.8 and ASASSN-V J101138.01−432812.6.

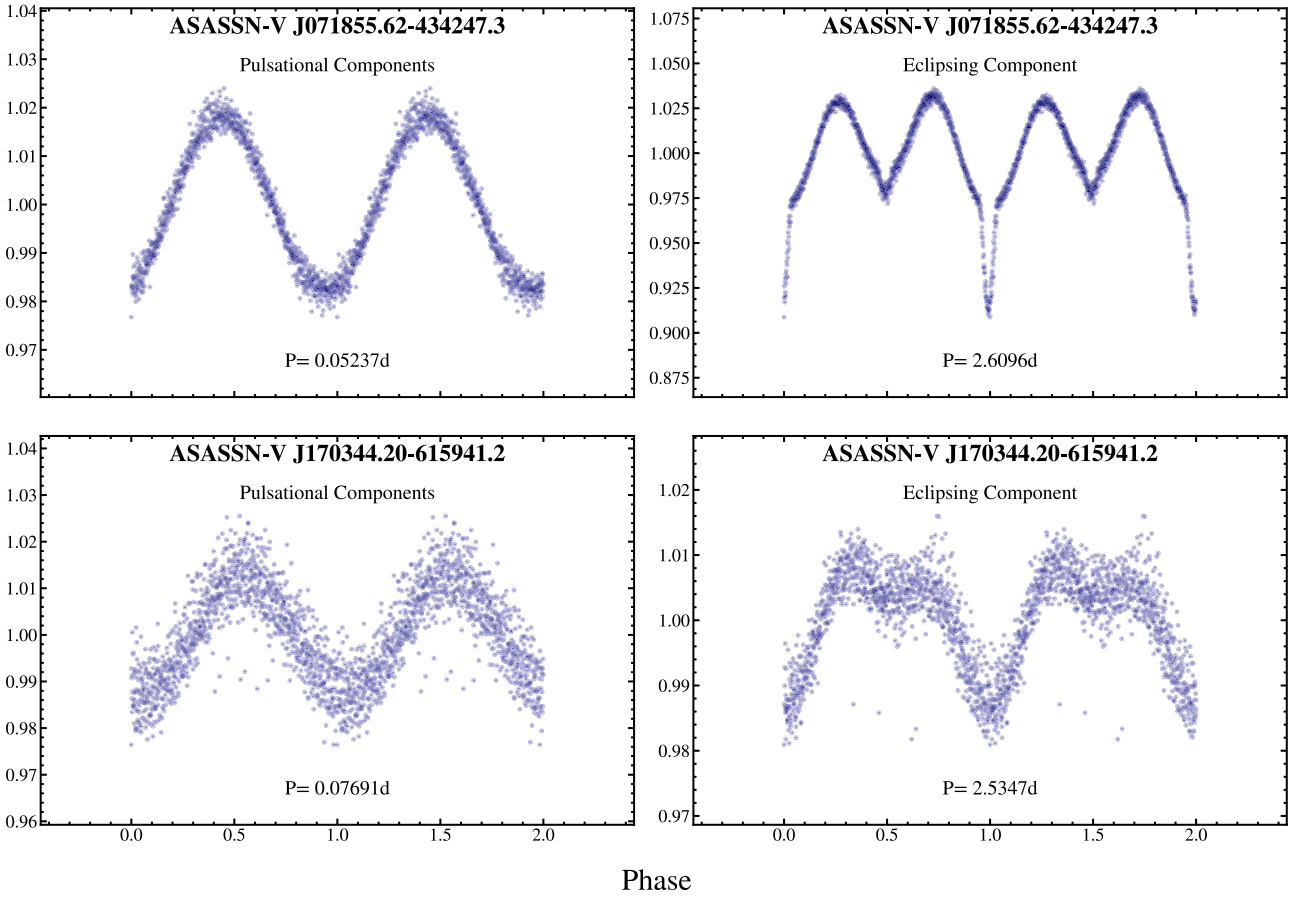

Figure 25. The pulsational (left) and eclipsing (right) components for the two eclipsing binaries ASASSN-V J071855.62−434247.3 and ASASSN-V J170344.20−615941.2 with a δ Scuti component. The format is the same as Fig. 23.

For the other overtone stars, we estimated the fundamental period $P_{\rm L}$ using the fundamental mode PLR and the W_{JK} magnitudes of these sources. The source ASASSN-V J071855.62−434247.3 is not included here, as the frequency analysis revealed only a single pulsation frequency after the removal of the binary orbital harmonics.

Expected period ratios for combinations of the fundamental mode and the first three overtone modes are highlighted (Stellingwerf 1979). Most of the overtone sources are clustered towards period ratios indicative of the second and third overtones. The overtone source ASASSN-V J084447.39−724126.6 appears to have $P_{\rm S}/P_{\rm L} \sim 0.42$, which is close to the possible period ratio for the fourth overtone identified in Fig. 7. Half of the fundamental mode sources appear to be multimode pulsators pulsating in the third overtone. The fundamental mode source ASASSN-V J173609.95−753309.6 has a very unusual period ratio of $P_{\rm S}/P_{\rm L} \sim 0.349$, which suggests that the frequency identified with $f_1 = 7.122\,998 {\rm d}^{-1}$ as $P_{\rm S}$ is a non-radial pulsation mode.

6 CONCLUSIONS

We analysed the all-sky catalogue of 8418 δ Scuti stars in the ASAS-SN *V*-band catalogue of variables, which includes 3322 new discoveries. We derive PLRs for fundamental mode and overtone δ Scuti stars in the W_{JK}, *V*, *Gaia* DR2 *G*, *J*, *H*, K_s, and W_1 bands. We identified a peak in the distribution of $\Delta \log P$ from the fundamental PLR fit corresponding to a period ratio of $P_{4O}/P_{\rm F} \sim 0.43$, which is likely to be the fourth overtone. We encourage a theoretical study of the fourth overtone mode in δ Scuti stars, as the empirical evidence points towards a population of δ Scuti stars pulsating with a dominant fourth overtone. We also investigated how the PLRs vary with the pulsational amplitude and *Gaia* DR2 distance, but did not find a significant variation in the PLRs with either parameter. The PLRs have shortcomings because the ASAS-SN photometric data and the period are not adequate to clearly separate all the mode sequences. This would be more feasible given a complete analysis of the *TESS* light curves.

We also cross-matched the catalogue to wide-field spectroscopic surveys, which resulted in 972 cross-matches. For the stars with spectroscopic parameters, we find that $T_{\rm eff}$ and $\log(g)$ are as expected from theoretical models. We used the calibrations in Torres et al. (2010) to derive masses and radii for these sources to find that the distributions of the radii of the fundamental mode and overtone pulsators were largely the same, but the distributions of masses were somewhat different, with an excess of overtone pulsators with masses $M > 1.8\,{\rm M}_{\odot}$ compared to the fundamental mode pulsators. An analysis of the pulsational constants (Q) for overtone pulsators in the spectroscopic sub-sample shows multiple peaks corresponding to the first, second, and third overtones visible in the data, and an absence of sources with Q close to the fundamental mode. This is in contrast to the fundamental mode pulsators that have Q values close to the expected value for the radial fundamental mode, and the first overtone. We again noted evidence for sources pulsating in the fourth overtone.

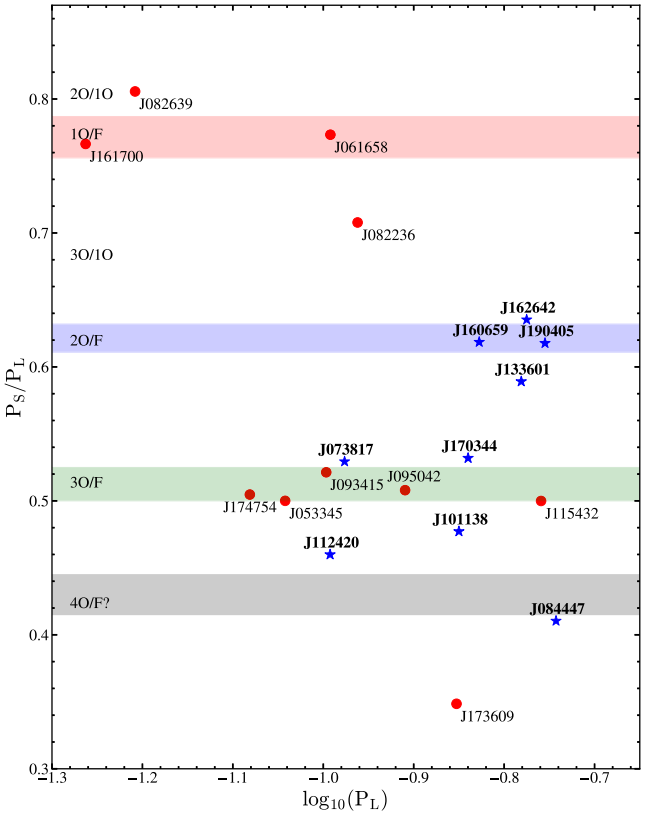

Figure 26. The Petersen diagram for the 10 fundamental mode and 10 overtone δ Scuti stars where we analysed the *TESS* light curves. The stars are identified through an abbreviated form of the ASAS-SN IDs listed in Table 3. Expected period ratios for combinations of the fundamental mode and the first three overtone modes are annotated (Stellingwerf 1979). The range of expected period ratios for δ Scuti stars pulsating in the fundamental mode and the first overtone (red), the second overtone (blue), or the third overtone (green) is shaded. The likely range of period ratios for the fourth overtone from Fig. 7 is shaded in black.

The periods of the fundamental mode δ Scuti stars vary with the metallicity, from $\log_{10}(P/\mathrm{days}) \sim -1.1$ for sources with [Fe/H] < -0.3 to $\log_{10}(P/\mathrm{days}) \sim -0.9$ for sources with supersolar metallicities [Fe/H] > 0. This leads to a period gradient with distance from the Galactic mid-plane. We find that δ Scuti stars with periods $P > 0.100$ d are predominantly located towards the Galactic disc ($|Z| < 0.5$ kpc). The median period at a scale height of $Z \sim 0$ kpc increases with the Galactocentric radius R, from $\log_{10}(P) \sim -0.94$ for sources with $R > 9$ kpc to $\log_{10}(P) \sim -0.85$ for sources with $R < 7$ kpc, which is indicative of a radial metallicity gradient.

As an experiment, we examined *TESS* light curves for a sample of 10 fundamental mode and 10 overtone δ Scuti stars discovered by ASAS-SN. A frequency analysis of these light curves showed that 19 of the 20 sources were multimode pulsators. Overtone sources had a dominant overtone mode and the expected fundamental mode was recovered in only two light curves. The analysis of the Petersen diagram showed that most of the overtone sources were clustered towards period ratios indicative of the second and third overtones, which is consistent with the analysis of the pulsational constants. We find that the unusual light curve of the source ASASSN-V J061658.98−213318.9 is composed of two dominant pulsation modes $f_0 = 9.820\,608\mathrm{d}^{-1}$ and $f_1 = 12.698\,695\mathrm{d}^{-1}$ with a period ratio $P_1/P_0 = 0.773$ that suggests that f_1 is the first overtone, and a remarkable array of high-amplitude beat frequencies. We also identified two new δ Scuti eclipsing binaries, ASASSN-V J071855.62−434247.3 and ASASSN-V J170344.20−615941.2, which were both in the sample of overtone pulsators, and have short orbital periods of $P_{\mathrm{orb}} = 2.6096$ d and $P_{\mathrm{orb}} = 2.5347$ d, respectively.

ACKNOWLEDGEMENTS

We thank the anonymous referee for the very useful comments that improved our presentation of this work. We thank Dr. Jennifer van Saders, Dr. Radoslaw Poleski, and Dr. Marc Pinsonneault for useful discussions on this manuscript. We thank the LCO and its staff for its continuing support of the ASAS-SN project. We also thank the Ohio State University College of Arts and Sciences Technology Services for helping us set up and maintain the ASAS-SN variable stars and photometry data bases.

ASAS-SN is supported by the Gordon and Betty Moore Foundation through grant GBMF5490 to the Ohio State University, and NSF grants AST-1515927 and AST-1908570. The development of ASAS-SN has been supported by NSF grant AST-0908816, the Mt. Cuba Astronomical Foundation, the Center for Cosmology and AstroParticle Physics at the Ohio State University, the Chinese Academy of Sciences South America Center for Astronomy (CASSACA), the Villum Foundation, and George Skestos.

KZS and CSK are supported by NSF grants AST-1515927, AST-1814440, and AST-1908570. This work is supported in part by Scialog Scholar grant 24216 from the Research Corporation. PJV is supported by the National Science Foundation Graduate Research Fellowship Program Under Grant No. DGE-1343012. BJS is supported by NSF grants AST-1908952, AST-1920392, and AST-1911074. TAT acknowledges support from a Simons Foundation Fellowship and from an IBM Einstein Fellowship from the Institute for Advanced Study, Princeton. Support for JLP is provided in part by the Ministry of Economy, Development, and Tourism's Millennium Science Initiative through grant IC120009, awarded to The Millennium Institute of Astrophysics, MAS. Support for OP has been provided by INTER-EXCELLENCE grant LTAUSA18093 from the Czech Ministry of Education, Youth, and Sports. The research of OP has also been supported by Horizon 2020 ERC Starting Grant 'Cat-In-hAT' (grant agreement #803158) and PRIMUS/SCI/17 award from Charles University. This work was partly supported by NSFC 11721303.

This paper includes data collected by the *TESS* mission, which are publicly available from the Mikulski Archive for Space Telescopes (MAST). Funding for the *TESS* mission is provided by NASA's Science Mission directorate.

We thank Ethan Kruse for uploading the TESS FFIs to YouTube, as these videos were invaluable when investigating the prevalence of scattered light artefacts for our targets.

This work has made use of data from the European Space Agency (ESA) mission *Gaia* (https://www.cosmos.esa.int/gaia), processed by the *Gaia* Data Processing and Analysis Consortium. This publication makes use of data products from the Two Micron All Sky Survey, as well as data products from the Wide-field Infrared Survey Explorer. This research was also made possible through the use of the AAVSO Photometric All-Sky Survey (APASS), funded by the Robert Martin Ayers Sciences Fund.

This research has made use of the VizieR catalogue access tool, CDS, Strasbourg, France. This research also made use of Astropy, a community-developed core Python package for Astronomy (Astropy Collaboration 2013).

REFERENCES

Aerts C., Christensen-Dalsgaard J., Kurtz D. W., 2010, Asteroseismology. Springer Netherlands, the Netherlands
Alard C., 2000, A&AS, 144, 363
Alard C., Lupton R. H., 1998, ApJ, 503, 325
Antoci V. et al., 2019, MNRAS, 490, 4040
Astropy Collaboration, 2013, A&A, 558, A33
Bailer-Jones C. A. L., Rybizki J., Fouesneau M., Mantelet G., Andrae R., 2018, AJ, 156, 58
Balona L. A., Dziembowski W. A., 2011, MNRAS, 417, 591
Beaton R. L. et al., 2018, Space Sci. Rev., 214, 113
Beaulieu J. P. et al., 1995, A&A, 303, 137
Bowman D. M., 2017, Amplitude Modulation of Pulsation Modes in Delta Scuti Stars, Springer Theses series. ISBN 978-3-319-66649-5. Springer Int. Publ., New York
Bowman D. M., Kurtz D. W., 2018, MNRAS, 476, 3169
Breger M., 1979, PASP, 91, 5
Breger M., 2000, in Michel B., Michael M., eds, ASP Conf. Ser. Vol. 210, Delta Scuti and Related Stars. Astron. Soc. Pac., San Francisco, p. 3
Breger M., Bregman J. N., 1975, ApJ, 200, 343
Breger M., McNamara B. J., Kerschbaum F., Huang L., Jiang S.-J., Guo S.-Z.-H., Poretti E., 1990, A&A, 231, 56
Breger M. et al., 1998, A&A, 331, 271
Breger M. et al., 1999, A&A, 349, 225
Brown T. M. et al., 2013, PASP, 125, 1031
Buder S. et al., 2018, MNRAS, 478, 4513
Cardelli J. A., Clayton G. C., Mathis J. S., 1989, ApJ, 345, 245
Casey A. R. et al., 2017, ApJ, 840, 59
Chang S.-W., Protopapas P., Kim D.-W., Byun Y.-I., 2013, AJ, 145, 132
Choi J., Dotter A., Conroy C., Cantiello M., Paxton B., Johnson B. D., 2016, ApJ, 823, 102
Cohen R. E., Sarajedini A., 2012, MNRAS, 419, 342
Cui X.-Q. et al., 2012, Res. Astron. Astrophys., 12, 1197
Cutri R. M. et al., 2013, VizieR Online Data Catalog, 2328
De Silva G. M. et al., 2015, MNRAS, 449, 2604
Dotter A., 2016, ApJS, 222, 8
Fausnaugh M. M. et al., 2019, preprint (arXiv:1904.02171)
Foreman-Mackey D., Hogg D. W., Lang D., Goodman J., 2013, PASP, 125, 306
Gaia Collaboration, 2018, A&A, 616, A1
Green G. M., 2018, J. Open Source Softw., 3, 695
Guzik J. A., Garcia J. A., Jackiewicz J., 2019, Frontiers Astron. Space Sci., 6, 40
Henden A. A., Levine S., Terrell D., Welch D. L., 2015, Am. Astron. Soc. Meeting Abstr., 225, 336.16
Hodapp K. W. et al., 2019, AJ, 158, 241
Holdsworth D. L. et al., 2014, MNRAS, 439, 2078
Holoien T. W.-S. et al., 2019, ApJ, 883, 111
Holtzman J. A. et al., 2015, AJ, 150, 148
Jaffe T. J., Barclay T., 2017, ticgen: A tool for calculating a TESS magnitude, and an expected noise level for stars to be observed by TESS, v1.0.0, Zenodo
Jayasinghe T. et al., 2018, MNRAS, 477, 3145
Jayasinghe T. et al., 2019a, MNRAS, 486, 1907
Jayasinghe T. et al., 2019b, MNRAS, 485, 961
Jayasinghe T. et al., 2019c, MNRAS, 489, 4705
Jayasinghe T. et al., 2019d, MNRAS, 491, 13
Kahraman Aliçavuş F., Soydugan E., Smalley B., Kubát J., 2017, MNRAS, 470, 915
Kochanek C. S. et al., 2017, PASP, 129, 104502
Lebzelter T., Mowlavi N., Marigo P., Pastorelli G., Trabucchi M., Wood P. R., Lecoeur-Taïbi I., 2018, A&A, 616, L13
Lenz P., Breger M., 2005, Commun. Asteroseismology, 146, 53
Madore B. F., 1982, ApJ, 253, 575
Majewski S. R. et al., 2017, AJ, 154, 94
McNamara D. H., 1995, AJ, 109, 1751
McNamara D., 1997, PASP, 109, 1221
McNamara D. H., 2000, in Michel B., Michael M., eds, ASP Conf. Ser. Vol. 210, Delta Scuti and Related Stars. Astron. Soc. Pac., San Francisco, p. 373
McNamara D. H., 2011, AJ, 142, 110
Morton T. D., 2015, Isochrones: Stellar Model Grid Package, Astrophysics Source Code Library, record ascl:1503.010
Murphy S. J., Hey D., Van Reeth T., Bedding T. R., 2019, MNRAS, 485, 2380
North P., Jaschek C., Egret D., 1997, ESA SP-402: Hipparcos - Venice 97. ESA, Noordwijk, p. 367
Pawlak M. et al., 2019, MNRAS, 487, 5932
Pedicelli S. et al., 2009, A&A, 504, 81
Pedregosa F. et al., 2012, preprint (arXiv:1201.0490)
Petersen J. O., 1973, A&A, 27, 89
Poleski R. et al., 2010, Acta Astron., 60, 1
Ricker G. R. et al., 2015, J. Astron. Telesc. Instrum. Syst., 1, 014003
Rodríguez E., Breger M., 2001, A&A, 366, 178
Sandage A., 1993, AJ, 106, 687
Scargle J. D., 1982, ApJ, 263, 835
Schlafly E. F., Finkbeiner D. P., 2011, ApJ, 737, 103
Schlegel D. J., Finkbeiner D. P., Davis M., 1998, ApJ, 500, 525
Shappee B. J. et al., 2014, ApJ, 788, 48
Skrutskie M. F. et al., 2006, AJ, 131, 1163
Stassun K. G. et al., 2018, AJ, 156, 102
Stellingwerf R. F., 1979, ApJ, 227, 935
Taylor M. B., 2005, in Shopbell P., Britton M., Ebert R., eds, ASP Conf. Ser. Vol. 347, Astronomical Data Analysis Software and Systems XIV. Astron. Soc. Pac., San Francisco, p. 29
Thompson T. A. et al., 2018, Science, 366, 637
Tonry J. L. et al., 2018, ApJ, 867, 105
Torres G., Andersen J., Giménez A., 2010, A&AR, 18, 67
Uytterhoeven K. et al., 2011, A&A, 534, A125
Vallely P. J. et al., 2019, MNRAS, 487, 2372
Vanderspek R. et al., 2018, TESS Instrument Handbook
Watson C. L., Henden A. A., Price A., 2006, Soc. Astron. Sci. 25th Annu. Symp. Telesc. Sci., Vol. 25, The International Variable Star Index (VSX). Soc. Astron. Sci., Rancho Cucamonga, CA, USA, p. 47
Wright E. L. et al., 2010, AJ, 140, 1868
Zechmeister M., Kürster M., 2009, A&A, 496, 577
Ziaali E., Bedding T. R., Murphy S. J., Van Reeth T., Hey D. R., 2019, MNRAS, 486, 4348

This paper has been typeset from a TEX/LATEX file prepared by the author.